Experimental and Modeling Study of Methyl Cyclohexane Pyrolysis and Oxidation

J. P. Orme, H. J. Curran,* and J. M. Simmie

Chemistry Department, National University of Ireland, Galway, Ireland

Received: August 5, 2005; In Final Form: September 29, 2005

Although the combustion chemistry of aliphatic hydrocarbons has been extensively documented, the oxidation of cyclic hydrocarbons has been studied to a much lesser extent. To provide a deeper understanding of the combustion chemistry of naphthenes, the oxidation of methylcyclohexane was studied in a series of high-temperature shock tube experiments. Ignition delay times for a series of mixtures, of varying methylcyclohexane/oxygen equivalence ratios ($\phi = 0.5$, 1.0, 2.0), were measured over reflected shock temperatures of 1200−2100 K and reflected shock pressures of 1.0, 2.0, and 4.0 atm. A detailed chemical kinetic mechanism has been assembled to simulate the shock tube results and flow reactor experiments, with good agreement observed.

Introduction

Much work has been carried out on the oxidation and pyrolysis of aliphatic hydrocarbons in a wide range of combustion environments. This research has provided an understanding of the kinetic pathways by which these fuels react under various conditions and has allowed the assembly of detailed chemical kinetic mechanisms[1] with considerable predictive powers.

However, the combustion chemistry of cyclic hydrocarbons has not been explored as extensively, with the possible exception of aromatics (benzene,[2−16] toluene,[17−24] and alkylbenzenes[25−28] receiving particular attention of late), whereas many naphthenes (cycloalkanes) have been neglected. There have been some studies on the oxidation of cyclohexane, cyclohexene, and cyclohexa-1,3-diene by Lemaire et al.[29] and Ribaucour et al.[30] and also the oxidation of cyclohexene by Dayma et al.[31]

Naphthenes are present in gasoline[32] and other fuels, emphasizing the need to provide a better understanding of their combustion properties. Some jet fuels, such as the JP-8 family, are composed mainly of monocyclic and bicyclic alkanes,[33] and up to 20% of Jet-A fuel, the commercial equivalent of JP-8, is also composed of cycloalkanes.[34] In addition to its role as a traditional fuel, methylcyclohexane (MCH) can provide a heat sink of up to 2190 kJ kg^{-1} through an endothermic dehydrogenation reaction, forming toluene, thus enhancing the cooling of jet engines, although the formation of aromatics may augment soot production and have a deleterious effect on the combustor liner.[35]

It is vital to understand the influence of the naphthene structure and the mixture composition on ignition delay times to control burning rates in homogeneous charge compression ignition engines and the "knocking" phenomenon in spark ignition engines.[36] MCH, with a research octane number of 75[37] and a cetane number of 20, is one naphthene for which there are very few experimental data available, and thus it is the focus of this work. Previous work includes a study of the unimolecular decomposition of MCH, as well as other methyl substituted cycloalkanes, using the technique of very low pressure pyrolysis at temperatures in the range 861−1218 K.[38] A rate constant for the dominant primary reaction channel of ring opening adjacent to the methyl substituent group of 2.51×10^{16} exp(−82457 cal mol^{-1}/RT) s^{-1} was reported.

A high temperature (1050−1200 K) turbulent flow reactor study[39] has been carried out on pure MCH and blends of MCH with toluene (one of its dehydrogenation products). MCH pyrolysis and oxidation decay profiles were determined at temperatures of 1058, 1108, 1154, and 1192 K, at atmospheric pressure. Species profiles were obtained over a 70 ms period for MCH oxidation at 1160 K and for MCH pyrolysis at 1155 K. Major products, for both oxidation and pyrolysis, included methane, ethylene, propene, buta-1,3-diene, and isoprene. Aromatics (benzene and toluene) were among the minor products as well as ethane, cyclopentadiene, cyclohexene, isobutene, allene, acetylene, and propyne.

Ignition delay times of MCH/O_2 mixtures were recorded behind incident shock waves by Hawthorn and Nixon,[40] in the temperature range 1200−1480 K, at equivalence ratios, ϕ, of 0.1−2.1, and pressures of 0.61, 1.02, and 1.70 atm. Most of the mixtures used, with the exceptions of $\phi = 0.1$ and 0.2, were very dilute blends of MCH and O_2 in 99% argon.

Granata et al.[41] performed a kinetic modeling study of the pyrolysis and oxidation of naphthenes, which allowed a semidetailed kinetic scheme to be expanded to incorporate the combustion properties of cyclohexane initially and was further extended to include MCH. This expansion was accomplished by adding the primary propagation reactions of cyclohexane and MCH to an existing mechanism, which had already been validated for the pyrolysis, partial oxidation, and combustion of hydrocarbons fuels such as *n*-heptane and isooctane.[42−44] Experimental species mole fractions from the turbulent flow reactor study[39] were used to verify the accuracy of the MCH mechanism, which was generally in good agreement with the experimental data. Moreover, this mechanism was used to simulate species profiles in laminar premixed flames for so-called surrogate mixtures of pure compounds that represent the aviation fuel JP-8.[34]

Specific Objectives

The aim of this study is to provide more information on the combustion characteristics of MCH and to develop a detailed chemical kinetic mechanism to enhance our knowledge of the pyrolysis and oxidation processes of naphthene fuels.

Experimental Section

The stainless steel shock tube consists of a large but short (52 cm diameter and 63 cm long) driver section coupled via a

10.1021/jp0543678 CCC: $33.50
Published on Web 12/13/2005

TABLE 1: Percent Composition of MCH/O_2/Ar Mixtures

ϕ	MCH	O_2	Ar
0.5	0.5	10.50	89.00
1.0	1.0	10.50	88.50
2.0	1.0	5.25	93.75
0.105	0.1	9.90	90.00

10 cm long transition piece to the test section that is 622 cm long and 10.24 cm internal diameter. Pressure transducers (PCB Piezotronics, model 113A21) were set into the final 50 cm of the test section and were used to measure the incident shock velocity with the aid of two universal time counters (HP5300A, TTi Apollo 100) and an oscilloscope (Tektronix TDS 2024). To allow for shock attenuation, the shock velocity at the endwall was calculated by extrapolating the incident velocities to the endwall. Reflected shock conditions were calculated, using the usual one-dimensional shock relations[45] and the application GasEq,[46] from initial temperatures in the range 290−298 K, and initial pressures in the range 12−107 Torr.

A polycarbonate diaphragm was allowed to burst under pressure with the assistance of a cross shaped cutting device that petaled the diaphragm. This shock tube was fully characterized[47] in line with a previous account[48] and validated against recent experiments on *n*-heptane oxidation from the Stanford group.[49]

Mixture Preparation. Test mixtures were prepared in a 50 L stainless steel tank using standard manometric methods. Gases were obtained from BOC Ireland Ltd.; helium CP Grade 99.999%, argon Zero Grade 99.998%, and oxygen Research Grade 99.985%. All gases were used without further purification. MCH was obtained from Aldrich Chemical Co. Ltd. and was determined to be 99.6% pure by GC analysis. To minimize the presence of atmospheric air in the sample, the liquid MCH was subjected to several freeze−pump−thaw degassing cycles before being used. The liquid MCH was incorporated into the mixing vessel by vaporization into the evacuated (10^{-6} Torr) mixing tank, and partial pressures were measured using a 100 Torr Baratron gauge to an accuracy of 0.01 Torr. Argon was added using a Wallace and Tiernan 800 Torr absolute pressure gauge. The exact composition of mixtures used during this study are shown in Table 1. Test gas mixtures were normally made up to a final pressure of 800 Torr and allowed to stand for 24 h to ensure homogeneity. From the resulting mix, initial pressures, p_1, varying from 12 to 107 Torr were used.

To test the consistency of this method, experiments were carried out on identical test gas mixtures that had been left standing for various lengths of time. There was no variation in the data produced using these mixtures.

Experimental Procedure. Prior to each experiment both the driver and driven sections of the shock tube were evacuated independently. The driver section was evacuated to 10^{-3} Torr using an Edwards oil rotary pump, whereas the driven section was first pumped to 10^{-3} Torr using an Edwards oil rotary pump, and the final pressure of 10^{-6} Torr was achieved using an Edwards oil diffusion pump.

Ignition Delay Time Measurements. Emissions were observed using an end on detection diagnostic that consisted of a PDA55 (switchable gain, amplified silicon detector) located behind a 431 nm (for CH* emission) narrow band-pass filter with a spectral bandwidth of 10 nm. The filter and the PDA were aligned behind a quartz window located in the endwall.

A Kistler pressure transducer, mounted flush with the endwall, signaled the shock wave arrival at the endwall, Figure 1, and the beginning of the ignition delay period. The end of the period was defined as the maximum rise in the rate of emission.

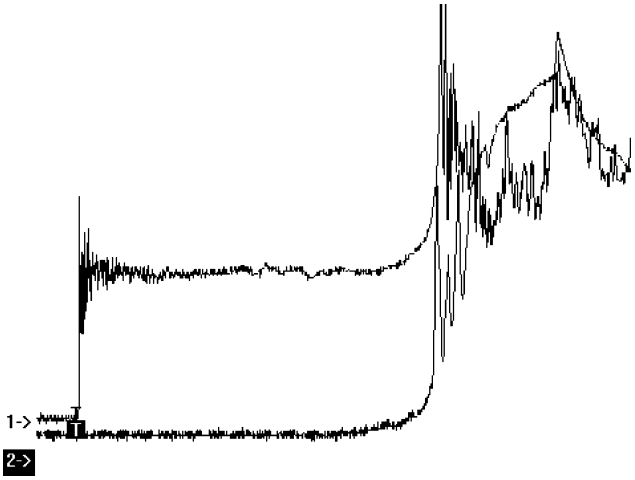

Figure 1. Typical endwall pressure sensor (1) and CH* emission (2) profiles. Conditions: 1.0% MCH, 10.5% O_2, 88.5% Ar, 1327.5 K, 2.0 atm.

A comparative study was carried out by repeating a series of shock tube experiments performed by Hawthorn and Nixon,[40] who defined ignition delay times as the length of time between shock arrival at the measurement plane, as indicated by a pressure transducer, and the first emission of light detected at the measurement plane. For these experiments the same end-on detection diagnostic was used, but the filter was removed to be consistent with the Hawthorn and Nixon study.

Simulated Ignition Delay Times and Species Profiles. The MCH oxidation mechanism was used, in conjunction with the Chemkin III suite of programs,[51] to simulate both the shock tube ignition delay times produced in this study and the flow reactor species profiles produced by Zeppieri et al.[39] Under the assumptions of constant pressure, uniform mixing and infinitely fast mass transport to the walls within the turbulent flow reactor, the Aurora module of Chemkin III was used to simulate the behavior of MCH under the experimental conditions of Zeppieri et al. The Shock module was used, with p_5 and T_5 supplied to the reflected shock mode, to simulate the ignition delays observed in this study.

For experimental ignition delays the end of the delay time was defined as the maximum rate of change of CH* emission. However, the mechanism used in this study, in common with most other mechanisms, does not contain the electronically excited CH* species. Horning et al.[50] states that the rate of emission can be inferred from the rate of production of CH*:

$$\dot{C}_2H + \dot{O} \rightarrow CH^* + CO$$

and defines the simulated ignition delay time as the time at which the maximum value of $[\dot{C}_2H][\dot{O}]$ occurs. This definition was used in this study.

Mechanism Formulation

The MCH mechanism is based on the reaction scheme developed by Laskin et al.,[52] which describes the oxidation of buta-1,3-diene, although the H_2/O_2 submechanism has been replaced with that recently published by Ó Conaire et al.[53] To this has been added the detailed chemistry that describes MCH oxidation and the oxidation of other intermediate hydrocarbon species larger than buta-1,3-diene. Rate constants for MCH oxidation are based on the analysis of Curran et al. for *n*-heptane[54] and isooctane[55] oxidation, in which a detailed description of reaction rate rules are described. Here we provide

TABLE 2: Thermodynamic Properties for Selected Species

species	$\Delta_f H°$(298 K)	$S°$(298 K)	C_p 300 K	400 K	500 K	600 K	800 K	1000 K	1500 K
MCH	−36.75	81.64	32.67	44.46	54.95	63.77	77.32	87.02	101.50
MCH[a]	−36.99	82.05	32.51	44.35	55.21	64.46	78.74	88.79	103.20
MCH-R1	7.65	86.88	31.89	41.98	51.40	59.62	72.57	82.00	96.11
MCH-R2	9.60	86.08	31.17	42.13	51.85	60.38	73.57	82.57	96.30
MCH-R3	9.60	86.08	31.17	42.13	51.85	60.38	73.57	82.57	96.30
MCH-R4	9.60	86.08	31.17	42.13	51.85	60.38	73.57	82.57	96.30
CYCHEXCH2	12.25	85.05	31.90	43.10	53.04	61.37	74.16	83.28	96.84

[a] MCH: $\Delta_f H°$ (kcal/mol) values from Prosen et al.,[56] $S°$ [cal/(mol K)] and C_p [cal/(mol K)] values from Beckett et al.[57]

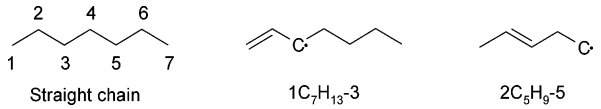

Figure 2. Naming scheme for straight chained hydrocarbons.

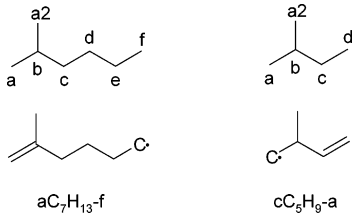

Figure 3. Naming scheme for branched hydrocarbons with a methyl group attached to the second carbon atom.

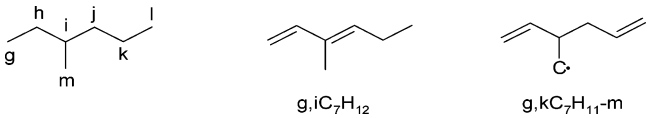

Figure 4. Naming scheme for branched hydrocarbons with a methyl group attached to the third carbon atom.

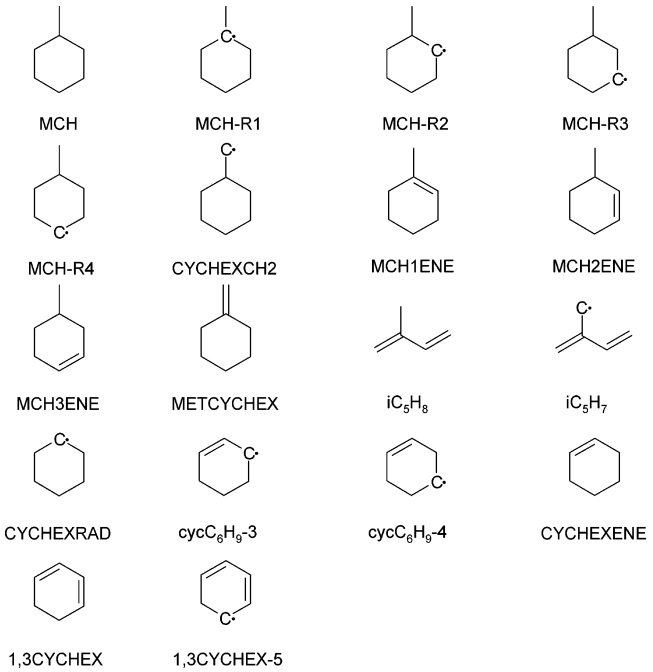

Figure 5. Names of miscellaneous hydrocarbons added to the MCH mechanism.

only details of updated rate constant expressions relative to those published for isooctane. Because so many rate expressions for MCH and its radical species have been derived using microscopic reversibility, the thermodynamic parameters of these species are included, Table 2; the thermodynamic values for MCH used in this study are in good agreement with previous work by Beckett et al.,[57] Table 2. These values have been determined using THERM[58] based on Benson's group additivity estimation method.[59] H/C/O groups and bond dissociation groups have been updated by taking into account the work of Lay et al.[60] and Sumathi and Green.[61] As the hydrogen/oxygen[53] and the buta-1,3-diene[52] submechanisms already appear in the literature, we have included only the methylcyclohexane submechanism, Table 3, where A is the pre-exponential frequency factor, n is the temperature curvature dependence, and E_a is the activation energy for reaction. A full listing of the detailed chemical kinetic mechanism is available in Chemkin format from the authors (henry.curran@nuigalway.ie).

Naming Scheme. Species names were created for use in Table 3 and Chemkin. To convert Table 3 to Chemkin format, an "X" was added before all species whose name began with a number and all commas and dashes were removed. Most species were given the notation "number-molecular formula-number" or "letter-molecular formula-letter". The numbers and letters can be explained as follows:

•For straight chain hydrocarbons the carbons were labeled with a number, starting with C1 upward along the chain, Figure 2.

•For branched hydrocarbons the carbons were labeled with a letter. For example, for 2-methylhexane the first carbon atom in the chain was labeled with an "a", the second with a "b" and so on, Figure 3. For 3-methylhexane the first atom was labeled with a "g" and so on, Figure 4.

•Where double bonds were present, numbers or letters were added before the molecular formula to denote their position on the hydrocarbon.

•Where radical sites were present, numbers or letters were added after the formula to denote their positions as shown, Figures 2−4.

Cyclic hydrocarbons and some branched species were given unique names that do not conform to the above naming schemes; these species are illustrated and named in Figure 5.

Species that were already present in the reaction scheme developed by Laskin et al., and the H_2/O_2 submechanism by Ó Conaire, were not renamed, with the exceptions of buta-1,3-diene, but-1-en-4-yl, and benzene, whose names were changed from C_4H_6 to $1,3C_4H_6$, $\dot{C}_4H_7$ to $1\dot{C}_4H_7$-4, and A1 to C_6H_6, respectively.

Unimolecular Fuel Decomposition. MCH decomposition can initiate through bond homolysis on the six-membered ring, leading to ring opening and the formation of C_7H_{14} diradical species. Bond homolysis can occur at six different sites with three unique diradicals being formed; homolysis of bonds that are equidistant from the methyl substituent lead to formation of equivalent species. The rate constant expressions used in this study for reactions of this type were consistent with those published by Brown and King in a very low pressure pyrolysis study of methyl- and ethynyl- cyclopentanes and cyclohexanes,

TABLE 3: Methylcyclohexane Mechanism Rate Coefficients; cm³/mol/s/cal Units

reaction	*A*	*n*	E_A
1. MCH = C_7H_{14}-g,l	2.5E+16	0.0	86042
2. MCH = C_7H_{14}-a,f	2.5E+16	0.0	86042
3. MCH = C_7H_{14}-1,6	2.5E+16	0.0	82457
4. CYCHEXRAD + CH_3 = MCH	6.63E+14	−0.6	0
5. $1C_6H_{11}$-6 = CYCHEXRAD	1.00E+08	0.9	5900
6. aC_7H_{13}-f = MCH-R1	1.00E+08	0.9	5900
7. gC_7H_{13}-l = MCH-R2	1.00E+08	0.9	5900
8. $2C_7H_{13}$-7 = MCH-R2	1.00E+08	0.9	8700
9. $1C_7H_{13}$-6 = MCH-R3	1.00E+08	0.9	8500
10. kC_7H_{13}-g = MCH-R3	1.00E+08	0.9	5900
11. eC_7H_{13}-a = MCH-R4	1.00E+08	0.9	5900
12. $1,3C_6H_9$-6 = $cycC_6H_9$-3	1.00E+08	0.9	6900
13. $1,4C_6H_9$-6 = $cycC_6H_9$-4	1.00E+08	0.9	6900
14. $1C_7H_{13}$-7 = CYCHEXCH2	1.00E+08	0.9	1903
15. $2C_6H_{10}$-1,6 = CYCHEXENE	1.00E+08	0.9	1000
16. $3C_6H_{10}$-1,6 = CYCHEXENE	1.00E+08	0.9	1000
17. aC_7H_{13}-f = aC_7H_{13}-c	3.67E+12	−0.6	15300
18. $1C_7H_{13}$-7 = $1C_7H_{13}$-3	2.80E+10	0.0	7500
19. gC_7H_{13}-l = gC_7H_{13}-i	3.67E+12	−0.6	13000
20. $2C_7H_{13}$-7 = $2C_7H_{13}$-4	3.67E+12	−0.6	15300
21. $2C_7H_{13}$-7 = $2C_7H_{13}$-1	2.80E+10	0.0	31640
22. $1C_7H_{13}$-6 = $1C_7H_{13}$-3	3.67E+12	−0.6	17900
23. kC_7H_{13}-g = kC_7H_{13}-j	3.67E+12	−0.6	15300
24. eC_7H_{13}-a = eC_7H_{13}-d	3.67E+12	−0.6	15300
25. $1C_6H_{11}$-6 = $1C_6H_{11}$-3	3.67E+12	−0.6	15300
26. C_7H_{14}-1,6 = $1C_7H_{14}$	3.67E+12	−0.6	15300
declared duplicate reaction...			
27. C_7H_{14}-1,6 = $1C_7H_{14}$	2.80E+10	0.0	25875
declared duplicate reaction...			
28. C_7H_{14}-1,6 = $2C_7H_{14}$	3.67E+12	−0.6	12800
29. C_7H_{14}-a,f = aC_7H_{14}	3.67E+12	−0.6	10500
30. C_7H_{14}-a,f = eC_7H_{14}	3.67E+12	−0.6	12800
31. C_7H_{14}-g,l = gC_7H_{14}	3.67E+12	−0.6	12800
32. C_7H_{14}-g,l = kC_7H_{14}	3.67E+12	−0.6	12800
33. $2C_5H_9$-5 = $2C_5H_9$-1	3.67E+12	−0.6	10000
34. $1C_5H_9$-4 = $1C_5H_9$-3	3.56E+10	0.9	31500
35. MCH + H = MCH-R1 + H_2	6.02E+05	2.4	2583
36. MCH + H = MCH-R2 + H_2	2.60E+06	2.4	4471
37. MCH + H = MCH-R3 + H_2	2.60E+06	2.4	4471
38. MCH + H = MCH-R4 + H_2	1.30E+06	2.4	4471
39. MCH + H = CYCHEXCH2 + H_2	6.65E+05	2.5	6756
40. MCH + CH_3 = MCH-R1 + CH_4	6.01E−10	6.4	893
41. MCH + CH_3 = MCH-R2 + CH_4	3.02E+00	3.5	5481
42. MCH + CH_3 = MCH-R3 + CH_4	3.02E+00	3.5	5481
43. MCH + CH_3 = MCH-R4 + CH_4	1.51E+00	3.5	5481
44. MCH + CH_3 = CYCHEXCH2 + CH_4	4.52E−01	3.6	7154
45. MCH + O_2 = MCH-R1 + HO_2	1.00E+13	0.0	48200
46. MCH + O_2 = MCH-R2 + HO_2	4.00E+13	0.0	49640
47. MCH + O_2 = MCH-R3 + HO_2	4.00E+13	0.0	49640
48. MCH + O_2 = MCH-R4 + HO_2	2.00E+13	0.0	49640
49. MCH + O_2 = CYCHEXCH2 + HO_2	3.00E+13	0.0	52290
50. MCH + HO_2 = MCH-R1 + H_2O_2	3.61E+03	2.5	10532
51. MCH + HO_2 = MCH-R2 + H_2O_2	1.93E+04	2.6	13910
52. MCH + HO_2 = MCH-R3 + H_2O_2	1.93E+04	2.6	13910
53. MCH + HO_2 = MCH-R4 + H_2O_2	9.64E+03	2.6	13910
54. MCH + HO_2 = CYCHEXCH2 + H_2O_2	2.38E+04	2.5	16494
55. MCH + OH = MCH-R1 + H_2O	5.73E+10	0.5	63
56. MCH + OH = MCH-R2 + H_2O	9.34E+07	1.6	−35
57. MCH + OH = MCH-R3 + H_2O	9.34E+07	1.6	−35
58. MCH + OH = MCH-R4 + H_2O	4.67E+07	1.6	−35
59. MCH + OH = CYCHEXCH2 + H_2O	5.27E+09	1.0	1586
60. MCH + CH_3O = MCH-R1 + CH_3OH	2.29E+10	0.0	2873
61. MCH + CH_3O = MCH-R2 + CH_3OH	2.90E+11	0.0	4571
62. MCH + CH_3O = MCH-R3 + CH_3OH	2.90E+11	0.0	4571
63. MCH + CH_3O = MCH-R4 + CH_3OH	1.45E+11	0.0	4571
64. MCH + CH_3O = CYCHEXCH2 + CH_3OH	2.17E+11	0.0	6458
65. MCH + O = MCH-R1 + OH	3.83E+05	2.4	1140
66. MCH + O = MCH-R2 + OH	1.10E+06	2.5	2830
67. MCH + O = MCH-R3 + OH	1.10E+06	2.5	2830
68. MCH + O = MCH-R4 + OH	5.51E+05	2.5	2830
69. MCH + O = CYCHEXCH2 + OH	9.80E+05	2.4	4750
70. $1,6C_7H_{12}$ + H = $1,6C_7H_{11}$-4 + H_2	1.30E+06	2.4	4471
71. $1,6C_7H_{12}$ + CH_3 = $1,6C_7H_{11}$-4 + CH_4	1.51E+00	3.5	5481
72. $1,6C_7H_{12}$ + O = $1,6C_7H_{11}$-4 + OH	5.51E+05	2.5	2830
73. $1,6C_7H_{12}$ + OH = $1,6C_7H_{11}$-4 + H_2O	4.67E+07	1.6	−35
74. iC_5H_8 + H = iC_5H_7 + H_2	1.73E+05	2.5	2492
75. iC_5H_8 + CH_3 = iC_5H_7 + CH_4	2.21E+00	3.5	5675
76. iC_5H_8 + OH = iC_5H_7 + H_2O	3.12E+06	2.0	−298
77. iC_5H_8 + HO_2 = iC_5H_7 + H_2O_2	9.64E+03	2.6	13910
78. iC_5H_8 + CH_3O = iC_5H_7 + CH_3OH	9.00E+01	3.0	11987
79. iC_5H_8 + O = iC_5H_7 + OH	4.41E+05	2.4	3150
80. iC_5H_8 + O_2 = iC_5H_7 + HO_2	3.30E+12	0.0	39900
81. CYCHEXENE + H = $cycC_6H_9$-3 + H_2	6.75E+05	2.4	207
82. CYCHEXENE + CH_3 = $cycC_6H_9$-3 + CH_4	7.38E+00	3.3	4002
83. CYCHEXENE + O = $cycC_6H_9$-3 + OH	1.32E+06	2.4	1210
84. CYCHEXENE + OH = $cycC_6H_9$-3 + H_2O	5.53E+04	2.6	−1919
85. CYCHEXENE + H = $cycC_6H_9$-4 + H_2	2.60E+06	2.4	4471
86. CYCHEXENE + CH_3 = $cycC_6H_9$-4 + CH_4	3.02E+00	3.5	5481
87. CYCHEXENE + O = $cycC_6H_9$-4 + OH	1.10E+06	2.5	2830
88. CYCHEXENE + OH = $cycC_6H_9$-4 + H_2O	9.34E+07	1.6	−35
89. a,eC_7H_{12} + H = a,eC_7H_{11}-c + H_2	3.38E+05	2.4	207
90. a,eC_7H_{12} + H = a,eC_7H_{11}-d + H_2	3.38E+05	2.4	207
91. $1,5C_7H_{12}$ + H = $1,5C_7H_{11}$-3 + H_2	3.38E+05	2.4	207
92. $1,5C_7H_{12}$ + H = $1,5C_7H_{11}$-4 + H_2	3.38E+05	2.4	207
93. g,kC_7H_{12} + H = g,kC_7H_{11}-j + H_2	3.38E+05	2.4	207
94. $1,4C_5H_8$ + H = $1,4C_5H_7$-3 + H_2	3.38E+05	2.4	207
95. a,eC_7H_{12} + CH_3 = a,eC_7H_{11}-c + CH_4	3.69E+00	3.3	4002
96. a,eC_7H_{12} + CH_3 = a,eC_7H_{11}-d + CH_4	3.69E+00	3.3	4002
97. $1,5C_7H_{12}$ + CH_3 = $1,5C_7H_{11}$-3 + CH_4	3.69E+00	3.3	4002
98. $1,5C_7H_{12}$ + CH_3 = $1,5C_7H_{11}$-4 + CH_4	3.69E+00	3.3	4002
99. g,kC_7H_{12} + CH_3 = g,kC_7H_{11}-j + CH_4	3.69E+00	3.3	4002
100. $1,4C_5H_8$ + CH_3 = $1,4C_5H_7$-3 + CH_4	3.69E+00	3.3	4002
101. a,eC_7H_{12} + O = a,eC_7H_{11}-c + OH	6.60E+05	2.4	1210
102. a,eC_7H_{12} + O = a,eC_7H_{11}-d + OH	6.60E+05	2.4	1210
103. $1,5C_7H_{12}$ + O = $1,5C_7H_{11}$-3 + OH	6.60E+05	2.4	1210
104. $1,5C_7H_{12}$ + O = $1,5C_7H_{11}$-4 + OH	6.60E+05	2.4	1210
105. g,kC_7H_{12} + O = g,kC_7H_{11}-j + OH	6.60E+05	2.4	1210
106. $1,4C_5H_8$ + O = $1,4C_5H_7$-3 + OH	6.60E+05	2.4	1210
107. a,eC_7H_{12} + OH = a,eC_7H_{11}-c + H_2O	2.76E+04	2.6	−1919
108. a,eC_7H_{12} + OH = a,eC_7H_{11}-d + H_2O	2.76E+04	2.6	−1919
109. $1,5C_7H_{12}$ + OH = $1,5C_7H_{11}$-3 + H_2O	2.76E+04	2.6	−1919
110. $1,5C_7H_{12}$ + OH = $1,5C_7H_{11}$-4 + H_2O	2.76E+04	2.6	−1919
111. g,kC_7H_{12} + OH = g,kC_7H_{11}-j + H_2O	2.76E+04	2.6	−1919
112. $1,4C_5H_8$ + OH = $1,4C_5H_7$-3 + H_2O	2.76E+04	2.6	−1919
113. $1,5C_6H_{10}$ + H = $1,5C_6H_9$-3 + H_2	6.75E+05	2.4	207
114. $1,5C_6H_{10}$ + CH_3 = $1,5C_6H_9$-3 + CH_4	7.38E+00	3.3	4002
115. $1,5C_6H_{10}$ + O = $1,5C_6H_9$-3 + OH	1.32E+06	2.4	1210
116. $1,5C_6H_{10}$ + OH = $1,5C_6H_9$-3 + H_2O	5.53E+04	2.6	−1919
117. $1,6C_7H_{12}$ + H = $1,6C_7H_{11}$-3 + H_2	6.75E+05	2.4	207
118. $1,6C_7H_{12}$ + CH_3 = $1,6C_7H_{11}$-3 + CH_4	7.38E+00	3.3	4002
119. $1,6C_7H_{12}$ + O = $1,6C_7H_{11}$-3 + OH	1.32E+06	2.4	1210
120. $1,6C_7H_{12}$ + OH = $1,6C_7H_{11}$-3 + H_2O	5.53E+04	2.6	−1919
121. $1,5C_7H_{12}$ + H = $1,5C_7H_{11}$-7 + H_2	1.73E+05	2.5	2492
122. $1,3C_5H_8$ + H = $1,3C_5H_75$ + H_2	1.73E+05	2.5	2492
123. a,eC_7H_{12} + H = a,eC_7H_{11}-a2 + H_2	1.73E+05	2.5	2492
124. $1,5C_7H_{12}$ + CH_3 = $1,5C_7H_{11}$-7 + CH_4	2.21E+00	3.5	5675
125. $1,3C_5H_8$ + CH_3 = $1,3C_5H_7$-5 + CH_4	2.21E+00	3.5	5675
126. a,eC_7H_{12} + CH_3 = a,eC_7H_{11}-a2 + CH_4	2.21E+00	3.5	5675
127. $1,5C_7H_{12}$ + O = $1,5C_7H_{11}$-7 + OH	4.41E+05	2.4	3150
128. $1,3C_5H_8$ + O = $1,3C_5H_7$-5 + OH	4.41E+05	2.4	3150
129. a,eC_7H_{12} + O = a,eC_7H_{11}-a2 + OH	4.41E+05	2.4	3150
130. $1,5C_7H_{12}$ + OH = $1,5C_7H_{11}$-7 + H_2O	3.12E+06	2.0	−298
131. $1,3C_5H_8$ + OH = $1,3C_5H_7$-5 + H_2O	3.12E+06	2.0	−298
132. a,eC_7H_{12} + OH = a,eC_7H_{11}-a2 + H_2O	3.12E+06	2.0	−298
133. g,kC_7H_{12} + H = g,kC_7H_{11}-m + H_2	6.65E+05	2.5	6756
134. g,kC_7H_{12} + CH_3 = g,kC_7H_{11}-m + CH_4	4.52E−01	3.6	7154
135. g,kC_7H_{12} + O = g,kC_7H_{11}-m + OH	9.80E+05	2.4	4750
136. g,kC_7H_{12} + OH = g,kC_7H_{11}-m + H_2O	5.27E+09	1.0	1586

TABLE 3: Continued

	reaction	*A*	*n*	E_A		reaction	*A*	*n*	E_A
137.	g,kC$_7$H$_{12}$ + H = g,kC$_7$H$_{11}$-i + H$_2$	2.65E+06	2.2	0	205.	MCH3ENE + H = MCH-R4	1.32E+13	0.0	3260
138.	g,kC$_7$H$_{12}$ + CH$_3$ = g,kC$_7$H$_{11}$-i + CH$_4$	4.61E+00	3.1	2330	206.	1,3C$_6$H$_{10}$ + H = 1C$_6$H$_{11}$-3	1.32E+13	0.0	3260
139.	g,kC$_7$H$_{12}$ + OH = g,kC$_7$H$_{11}$-i + H$_2$O	6.14E+02	3.2	−3500	207.	a,cC$_7$H$_{12}$ + H = aC$_7$H$_{13}$-c	1.32E+13	0.0	3260
140.	1C$_7$H$_{14}$ + H = 1C$_7$H$_{13}$-3 + H$_2$	3.38E+05	2.4	207	208.	1,3C$_7$H$_{12}$ + H = 1C$_7$H$_{13}$-3	1.32E+13	0.0	3260
141.	1C$_7$H$_{14}$ + CH$_3$ = 1C$_7$H$_{13}$-3 + CH$_4$	3.69E+00	3.3	4002	209.	g,iC$_7$H$_{12}$ + H = gC$_7$H$_{13}$-i	1.32E+13	0.0	3260
142.	1C$_7$H$_{14}$ + OH = 1C$_7$H$_{13}$-3 + H$_2$O	2.76E+04	2.6	−1919	210.	2,4C$_7$H$_{12}$ + H = 2C$_7$H$_{13}$-4	1.32E+13	0.0	3260
143.	1C$_7$H$_{14}$ + HO$_2$ = 1C$_7$H$_{13}$-3 + H$_2$O$_2$	4.82E+03	2.5	10532	211.	c,eC$_7$H$_{12}$ + H = eC$_7$H$_{13}$-d	1.32E+13	0.0	3260
144.	1C$_7$H$_{14}$ + CH$_3$O = 1C$_7$H$_{13}$-3 + CH$_3$OH	4.00E+01	2.9	8609	212.	1,3CYCHEX + H = cycC$_6$H$_9$-4	1.32E+13	0.0	3260
145.	1C$_7$H$_{14}$ + O = 1C$_7$H$_{13}$-3 + OH	6.60E+05	2.4	1210	213.	1,4CYCHEX + H = cycC$_6$H$_9$-4	1.32E+13	0.0	3260
146.	1C$_7$H$_{14}$ + O$_2$ = 1C$_7$H$_{13}$-3 + HO$_2$	2.20E+12	0.0	37220	214.	1,3C$_5$H$_8$ + H = 2C$_5$H$_9$-1	1.32E+13	0.0	3260
147.	2C$_7$H$_{14}$ + H = 2C$_7$H$_{13}$-1 + H$_2$	1.73E+05	2.5	2492	215.	aC$_7$H$_{13}$-f + H = C$_7$H$_{14}$-a,f	1.32E+13	0.0	4660
148.	2C$_7$H$_{14}$ + H = 2C$_7$H$_{13}$-4 + H$_2$	3.38E+05	2.4	207	216.	a,eC$_7$H$_{12}$ + H = eC$_7$H$_{13}$-a	1.32E+13	0.0	4660
149.	2C$_7$H$_{14}$ + CH$_3$ = 2C$_7$H$_{13}$-1 + CH$_4$	4.52E−01	3.6	7154	217.	iC$_5$H$_8$ + H = cC$_5$H$_9$-a	1.32E+13	0.0	4660
150.	2C$_7$H$_{14}$ + CH$_3$ = 2C$_7$H$_{13}$-4 + CH$_4$	3.69E+00	3.3	4002	218.	g,k,mC$_7$H$_{10}$ + H = g,kC$_7$H$_{11}$-m	1.32E+13	0.0	4660
151.	2C$_7$H$_{14}$ + O = 2C$_7$H$_{13}$-1 + OH	4.41E+05	2.4	3150	219.	g,i,kC$_7$H$_{10}$ + H = g,kC$_7$H$_{11}$-j	1.32E+13	0.0	4660
152.	2C$_7$H$_{14}$ + OH = 2C$_7$H$_{13}$-1 + H$_2$O	3.12E+06	2.0	−298	220.	METCYCHEX + H = CYCHEXCH2	1.32E+13	0.0	4660
153.	2C$_7$H$_{14}$ + O = 2C$_7$H$_{13}$-4 + OH	6.60E+05	2.4	1210	221.	MCH1ENE + H = MCH-R2	1.32E+13	0.0	4660
154.	2C$_7$H$_{14}$ + OH = 2C$_7$H$_{13}$-4 + H$_2$O	2.76E+04	2.6	−1919	222.	i,kC$_7$H$_{12}$ + H = kC$_7$H$_{13}$-j	1.32E+13	0.0	4660
155.	aC$_7$H$_{14}$ + H = aC$_7$H$_{13}$-c + H$_2$	3.38E+05	2.4	207	223.	1C$_7$H$_{13}$-7 + H = C$_7$H$_{14}$-1,6	2.64E+13	0.0	2160
156.	aC$_7$H$_{14}$ + CH$_3$ = aC$_7$H$_{13}$-c + CH$_4$	3.69E+00	3.3	4002	224.	1,6C$_7$H$_{12}$ + H = 1C$_7$H$_{13}$-6	2.64E+13	0.0	2160
157.	aC$_7$H$_{14}$ + O = aC$_7$H$_{13}$-c + OH	6.60E+05	2.4	1210	225.	1,3C$_5$H$_8$ + H = 1C$_5$H$_9$-4	2.64E+13	0.0	2160
158.	aC$_7$H$_{14}$ + OH = aC$_7$H$_{13}$-c + H$_2$O	2.76E+04	2.6	−1919	226.	g,k,mC$_7$H$_{10}$ + H = g,k-C$_7$H$_{11}$-i	2.64E+13	0.0	2160
159.	eC$_7$H$_{14}$ + H = eC$_7$H$_{13}$-d + H$_2$	3.38E+05	2.4	207	227.	METCYCHEX + H = MCH-R1	2.64E+13	0.0	2160
160.	eC$_7$H$_{14}$ + CH$_3$ = eC$_7$H$_{13}$-d + CH$_4$	3.69E+00	3.3	4002	228.	g,mC$_7$H$_{12}$ + H = gC$_7$H$_{13}$-i	2.64E+13	0.0	2160
161.	eC$_7$H$_{14}$ + O = eC$_7$H$_{13}$-d + OH	6.60E+05	2.4	1210	229.	1C$_4$H$_7$-4 + C$_2$H$_4$ = 1C$_6$H$_{11}$-6	1.32E+04	2.5	6130
162.	eC$_7$H$_{14}$ + OH = eC$_7$H$_{13}$-d + H$_2$O	2.76E+04	2.6	−1919	230.	2C$_5$H$_9$-5 + C$_2$H$_4$ = 2C$_7$H$_{13}$-7	1.32E+04	2.5	6130
163.	gC$_7$H$_{14}$ + H = gC$_7$H$_{13}$-i + H$_2$	2.65E+06	2.2	0	231.	1C$_5$H$_9$-5 + C$_2$H$_4$ = 1C$_7$H$_{13}$-7	1.32E+04	2.5	6130
164.	gC$_7$H$_{14}$ + CH$_3$ = gC$_7$H$_{13}$-i + CH$_4$	4.61E+00	3.1	2330	232.	aC$_5$H$_9$-d + C$_2$H$_4$ = aC$_7$H$_{13}$-f	1.32E+04	2.5	6130
165.	gC$_7$H$_{14}$ + OH = gC$_7$H$_{13}$-i + H$_2$O	6.14E+02	3.2	−3500	233.	cC$_5$H$_9$-a + C$_2$H$_4$ = gC$_7$H$_{13}$-l	1.32E+04	2.5	6130
166.	kC$_7$H$_{14}$ + H = kC$_7$H$_{13}$-j + H$_2$	3.38E+05	2.4	207	234.	C$_2$H$_4$ + aC$_3$H$_5$ = 1C$_5$H$_9$-5	1.32E+04	2.5	6130
167.	kC$_7$H$_{14}$ + CH$_3$ = kC$_7$H$_{13}$-j + CH$_4$	3.69E+00	3.3	4002	235.	C$_2$H$_4$ + sC$_3$H$_5$ = 2C$_5$H$_9$-5	1.32E+04	2.5	6130
168.	kC$_7$H$_{14}$ + O = kC$_7$H$_{13}$-j + OH	6.60E+05	2.4	1210	236.	C$_2$H$_4$ + tC$_3$H$_5$ = aC$_5$H$_9$-d	1.32E+04	2.5	6130
169.	kC$_7$H$_{14}$ + OH = kC$_7$H$_{13}$-j + H$_2$O	2.76E+04	2.6	−1919	237.	C$_2$H$_4$ + *n*-C$_4$H$_5$ = 1,3C$_6$H$_9$-6	1.32E+04	2.5	6130
170.	CYCHEXENE + H = CYCHEXRAD	1.32E+13	0.0	3260	238.	1C$_5$H$_9$-4 + C$_2$H$_4$ = kC$_7$H$_{13}$-g	1.32E+04	2.5	6130
171.	1,5C$_6$H$_{10}$ + H = 1C$_6$H$_{11}$-6	1.32E+13	0.0	3260	239.	C$_5$H$_{10}$-1,4 + C$_2$H$_4$ = C$_7$H$_{14}$-1,6	1.32E+04	2.5	6130
172.	1C$_7$H$_{13}$-6 + H = C$_7$H$_{14}$-1,6	1.32E+13	0.0	3260	240.	C$_5$H$_{10}$-a,d + C$_2$H$_4$ = C$_7$H$_{14}$-a,f	1.32E+04	2.5	6130
173.	2C$_7$H$_{13}$-7 + H = C$_7$H$_{14}$-1,6	1.32E+13	0.0	3260	241.	C$_5$H$_{10}$-1,4 + C$_2$H$_4$ = C$_7$H$_{14}$-g,l	1.32E+04	2.5	6130
174.	1,5C$_7$H$_{12}$ + H = 1C$_7$H$_{13}$-6	1.32E+13	0.0	3260	242.	C$_5$H$_{10}$-a,d + C$_2$H$_4$ = C$_7$H$_{14}$-g,l	1.32E+04	2.5	6130
175.	1,5C$_7$H$_{12}$ + H = 2C$_7$H$_{13}$-7	1.32E+13	0.0	3260	243.	C$_3$H$_6$ + 1C$_4$H$_7$-4 = 1C$_7$H$_{13}$-6	8.80E+03	2.5	6130
176.	1,6C$_7$H$_{12}$ + H = 1C$_7$H$_{13}$-7	1.32E+13	0.0	3260	244.	1C$_4$H$_7$-4 + C$_3$H$_6$ = eC$_7$H$_{13}$-a	8.80E+03	2.5	6130
177.	eC$_7$H$_{13}$-a + H = C$_7$H$_{14}$-a,f	1.32E+13	0.0	3260	245.	C$_3$H$_6$ + C$_2$H$_3$ = 1C$_5$H$_9$-4	8.80E+03	2.5	6130
178.	a,eC$_7$H$_{12}$ + H = aC$_7$H$_{13}$-f	1.32E+13	0.0	3260	246.	1,3C$_4$H$_6$ + aC$_3$H$_5$ = 1,5C$_7$H$_{11}$-7	8.80E+03	2.5	6130
179.	gC$_7$H$_{13}$-l + H = C$_7$H$_{14}$-g,l	1.32E+13	0.0	3260	247.	1,3C$_4$H$_6$ + C$_2$H$_5$ = 1C$_6$H$_{11}$-3	8.80E+03	2.5	6130
180.	kC$_7$H$_{13}$-g + H = C$_7$H$_{14}$-g,l	1.32E+13	0.0	3260	248.	iC$_5$H$_8$ + C$_2$H$_5$ = aC$_7$H$_{13}$-c	8.80E+03	2.5	6130
181.	iC$_5$H$_8$ + H = aC$_5$H$_9$-d	1.32E+13	0.0	3260	249.	1,3C$_4$H$_6$ + nC$_3$H$_7$ = 1C$_7$H$_{13}$-3	8.80E+03	2.5	6130
182.	g,kC$_7$H$_{12}$ + H = gC$_7$H$_{13}$-l	1.32E+13	0.0	3260	250.	iC$_5$H$_8$ + C$_2$H$_5$ = gC$_7$H$_{13}$-i	8.80E+03	2.5	6130
183.	g,kC$_7$H$_{12}$ + H = kC$_7$H$_{13}$-g	1.32E+13	0.0	3260	251.	1,3C$_5$H$_8$ + C$_2$H$_5$ = 2C$_7$H$_{13}$-4	8.80E+03	2.5	6130
184.	1,4C$_5$H$_8$ + H = 1C$_5$H$_9$-5	1.32E+13	0.0	3260	252.	tC$_3$H$_5$ + 1,3C$_4$H$_6$ = a,eC$_7$H$_{11}$-d	8.80E+03	2.5	6130
185.	1,4C$_5$H$_8$ + H = 1C$_5$H$_9$-4	1.32E+13	0.0	3260	253.	1,3C$_4$H$_6$ + iC$_3$H$_7$ = eC$_7$H$_{13}$-d	8.80E+03	2.5	6130
186.	1,3C$_5$H$_8$ + H = 2C$_5$H$_9$-5	1.32E+13	0.0	3260	254.	1,3C$_4$H$_6$ + C$_2$H$_3$ = 1,4C$_6$H$_9$-6	8.80E+03	2.5	6130
187.	C$_3$H$_6$ + C$_2$H$_3$ = cC$_5$H$_9$-a	1.32E+13	0.0	3260	255.	1,3C$_4$H$_6$ + C$_2$H$_3$ = 1,5C$_6$H$_9$-3	8.80E+03	2.5	6130
188.	1,3,6C$_7$H$_{10}$ + H = 1,6C$_7$H$_{11}$-3	1.32E+13	0.0	3260	256.	1,4C$_5$H$_8$ + C$_2$H$_3$ = 1,6C$_7$H$_{11}$-4	8.80E+03	2.5	6130
189.	1,3,5C$_6$H$_8$ + H = 1,5C$_6$H$_9$-3	1.32E+13	0.0	3260	257.	1,3C$_4$H$_6$ + sC$_3$H$_5$ = 1,5C$_7$H$_{11}$-3	8.80E+03	2.5	6130
190.	1,3,6C$_7$H$_{10}$ + H = 1,6C$_7$H$_{11}$-4	1.32E+13	0.0	3260	258.	C$_2$H$_3$ + 1,3C$_5$H$_8$ = 1,5C$_7$H$_{11}$-4	8.80E+03	2.5	6130
191.	1,3,5C$_7$H$_{10}$ + H = 1,5C$_7$H$_{11}$-3	1.32E+13	0.0	3260	259.	C$_2$H$_3$ + 1,4-C$_5$H$_8$ = g,kC$_7$H$_{11}$-m	8.80E+03	2.5	6130
192.	1,3,5C$_7$H$_{10}$ + H = 1,5C$_7$H$_{11}$-4	1.32E+13	0.0	3260	260.	iC$_5$H$_8$ + C$_2$H$_3$ = a,eC$_7$H$_{11}$-c	8.80E+03	2.5	6130
193.	1,3,6C$_7$H$_{10}$ + H = 1,5C$_7$H$_{11}$-7	1.32E+13	0.0	3260	261.	1,3C$_4$H$_6$ + aC$_3$H$_5$ = 1,6C$_7$H$_{11}$-4	8.80E+03	2.5	6130
194.	a,c,eC$_7$H$_{10}$ + H = a,eC$_7$H$_{11}$-c	1.32E+13	0.0	3260	262.	1,3C$_4$H$_6$ + aC$_3$H$_5$ = 1,6C$_7$H$_{11}$-3	8.80E+03	2.5	6130
195.	a,c,eC$_7$H$_{10}$ + H = a,eC$_7$H$_{11}$-d	1.32E+13	0.0	3260	263.	1,3C$_4$H$_6$ + aC$_3$H$_5$ = g,kC$_7$H$_{11}$-m	8.80E+03	2.5	6130
196.	1,3CYCHEX + H = cycC$_6$H$_9$-3	1.32E+13	0.0	3260	264.	1,3C$_4$H$_6$ + aC$_3$H$_5$ = g,kC$_7$H$_{11}$-i	8.80E+03	2.5	6130
197.	1,3,5C$_6$H$_8$ + H = 1,3C$_6$H$_9$-6	1.32E+13	0.0	3260	265.	C$_4$H$_8$-1,4 + C$_3$H$_6$ = C$_7$H$_{14}$-1,6	8.80E+03	2.5	6130
198.	1,3,5C$_6$H$_8$ + H = 1,4C$_6$H$_9$-6	1.32E+13	0.0	3260	266.	1,3C$_4$H$_6$ + nC$_3$H$_7$ = 2C$_7$H$_{13}$-1	8.80E+03	2.5	6130
199.	1,4C$_6$H$_9$-6 + H = 2C$_6$H$_{10}$-1,6	1.32E+13	0.0	3260	267.	1C$_6$H$_{11}$-6 + CH$_3$ = C$_7$H$_{14}$-a,f	1.89E+03	2.7	6850
200.	1,3C$_6$H$_9$-6 + H = 3C$_6$H$_{10}$-1,6	1.32E+13	0.0	3260	268.	1,5C$_6$H$_{10}$ + CH$_3$ = eC$_7$H$_{13}$-a	1.89E+03	2.7	6850
201.	MCH1ENE + H = MCH-R1	1.32E+13	0.0	3260	269.	1,3C$_4$H$_6$ + CH$_3$ = cC$_5$H$_9$-a	1.89E+03	2.7	6850
202.	MCH2ENE + H = MCH-R2	1.32E+13	0.0	3260	270.	1,3,5C$_6$H$_8$ + CH$_3$ = g,kC$_7$H$_{11}$-j	1.89E+03	2.7	6850
203.	MCH2ENE + H = MCH-R3	1.32E+13	0.0	3260	271.	CYCHEXENE + CH$_3$ = MCH-R2	1.89E+03	2.7	6850
204.	MCH3ENE + H = MCH-R3	1.32E+13	0.0	3260	272.	1,3C$_6$H$_{10}$ + CH$_3$ = kC$_7$H$_{13}$-j	1.89E+03	2.7	6850

TABLE 3: Continued

	reaction	*A*	*n*	E_A		reaction	*A*	*n*	E_A
273.	$1,2,5C_6H_8 + CH_3 = a,eC_7H_{11}$-c	1.89E+03	2.7	6850	286.	$C_2H_4 + C_2H_4 = C_4H_8$-1,4	6.63E+14	−0.6	0
274.	$1,3C_4H_6 + CH_3 = 2C_5H_9$-1	1.76E+04	2.5	6130	287.	$C_2H_4 + C_3H_6 = C_5H_{10}$-1,4	6.63E+14	−0.6	0
275.	$1,3C_4H_6 + CH_3 = 1C_5H_9$-3	1.76E+04	2.5	6130	288.	$aC_3H_5 + C_4H_91 = 1C_7H_{14}$	6.63E+14	−0.6	0
276.	$C_2H_3 + aC_3H_4 = iC_5H_7$	9.45E+02	2.7	6850	289.	$1C_4H_7$-4 + $nC_3H_7 = 1C_7H_{14}$	6.63E+14	−0.6	0
277.	$1,3C_5H_8 + C_2H_5 = kC_7H_{13}$-j	9.45E+02	2.7	6850	290.	$1C_5H_9$-5 + $C_2H_5 = 1C_7H_{14}$	6.63E+14	−0.6	0
278.	$aC_3H_4 + 1C_4H_7$-4 = a,eC_7H_{11}-a2	9.45E+02	2.7	6850	291.	$nC_4H_5 + CH_3 = 1,3C_5H_8$	6.63E+14	−0.6	0
279.	C_4H_8-1,4 + $C_3H_6 = C_7H_{14}$-a,f	9.45E+02	2.7	6850	292.	CYCHEXENE = $1,3C_4H_6 + C_2H_4$	3.64E+62	−13.8	92030
280.	$aC_3H_5 + aC_3H_5 = 1,5C_6H_{10}$	6.63E+14	−0.6	0	293.	1,3CYCHEX = $C_6H_6 + H_2$	2.36E+19	−1.4	67530
281.	$aC_3H_5 + 1C_4H_7$-4 = $1,6C_7H_{12}$	6.63E+14	−0.6	0	294.	1,3CYCHEX = 1,3CYCHEX-5 + H	5.01E+15	0.0	72600
282.	$aC_3H_5 + iC_4H_7 = 1,5C_7H_{12}$	6.63E+14	−0.6	0	295.	1,3CYCHEX-5 = C_6H_6 + H	4.80E+25	−3.5	33480
283.	$iC_4H_7 + aC_3H_5 = g,kC_7H_{12}$	6.63E+14	−0.6	0	296.	1,3CYCHEX-5 = $nC_4H_5 + C_2H_2$	2.51E+14	0.7	41827
284.	$1,5C_6H_9$-3 + $CH_3 = g,kC_7H_{12}$	6.63E+14	−0.6	0	297.	$2C_6H_{10}$-1,6 = $1,3C_4H_6 + C_2H_4$	2.07E+13	0.4	38219
285.	$iC_4H_5 + CH_3 = iC_5H_8$	6.63E+14	−0.6	0	298.	$3C_6H_{10}$-1,6 = $C_2H_4 + C_2H_2 + C_2H_4$	2.07E+13	0.4	38219

TABLE 4: MCH Decomposition Forming Diradicals; s/cal/mol Units

radical type	*A*	*n*	E_A
MCH → C_7H_{14}-1,6	2.5E+16	0.0	82457
MCH → C_7H_{14}-a,f	2.5E+16	0.0	86042
MCH → C_7H_{14}-g,l	2.5E+16	0.0	86042

TABLE 5: Arrhenius Parameters per H-Atom; cm³/mol/s/cal Units

abstraction by	C-type	*A*	*n*	E_A
Ḣ	1°	2.22E+05	2.54	6756
	2°	6.50E+05	2.40	4471
	3°	6.02E+05	2.40	2583
ȮH	1°	1.76E+09	0.97	1586
	2°	2.34E+07	1.61	−35
	3°	5.73E+10	0.51	63
$\dot{C}H_3$	1°	1.51E−01	3.65	7154
	2°	7.55E−01	3.46	5481
	3°	6.01E−10	6.36	893
$H\dot{O}_2$	1°	7.93E+03	2.55	16 494
	2°	4.82E+03	2.60	13 910
	3°	3.61E+03	2.55	10 532
$CH_3\dot{O}_2$	1°	7.93E+03	2.55	16 494
	2°	4.82E+03	2.60	13 910
	3°	3.61E+03	2.55	10 532
$CH_3\dot{O}$	1°	7.23E+10	0.00	6458
	2°	7.25E+10	0.00	4571
	3°	2.29E+10	0.00	2873
Ȯ	1°	3.27E+05	2.43	4750
	2°	2.76E+05	2.45	2830
	3°	3.83E+05	2.41	1140
O_2	1°	1.00E+13	0.00	52 290
	2°	1.00E+13	0.00	49 640
	3°	1.00E+13	0.00	48 200

Table 4.[38] The authors estimated rate expressions and compared simulated MCH decomposition profiles to their experimental raw data with satisfactory agreement. Their estimations were based on known values for the corresponding carbon carbon bond fissions in open chain alkanes and are in good agreement with the literature.

The reaction forming a cyclohexyl (CYCHEXRAD), Figure 5, and a methyl radical was determined using the reverse recombination rate constant of $6.63 \times 10^{14}T^{-0.57}$ cm³ mol^{-1} s^{-1} taken from the work of Tsang[63] for methyl addition to an isopropyl radical and then calculated using microscopic reversibility.

Hydrogen Atom Abstraction. Hydrogen atom abstraction from MCH takes place at primary, secondary, and tertiary sites. Rate constant expressions for site-specific hydrogen atom abstraction reactions by various radicals have been published previously.[54,55,64] However, these values are continually being updated and, hence, slightly different values were used in this study and are reported in Table 5.

TABLE 6: Ċ Radical Addition; cm³/mol/s/cal Units

radical type	*A*	*n*	E_A
External Ċ Radical Addition			
$\dot{C}H_3 + 1,3C_4H_6$	1.76E+04	2.48	6130
$\dot{C}_2H_5$ (or larger) + C_2H_4	1.32E+04	2.48	6130
$\dot{C}_2H_5$ (or larger) + C_3H_6 (or larger)	8.80E+03	2.48	6130
Internal Ċ Radical Addition			
$\dot{C}H_3 + C_3H_6$ (or larger)	1.89E+03	2.67	6850
$\dot{C}_2H_5$ (or larger) + C_3H_6 (or larger)	9.45E+02	2.67	6850

Alkyl Radical Decomposition. The rate constants for alkyl radical decomposition were estimated in the reverse, exothermic direction, that is, the addition of an alkyl radical to an alkene. These expressions are taken from a study by Curran[65] for C_1−C_4 alkyl and alkoxyl radical decompositions, Table 6.

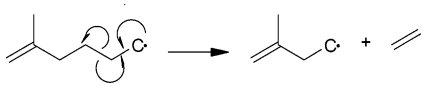

The decomposition of 2-methylhex-1-en-6-yl ($a\dot{C}_7H_{13}$-f) radical to form ethylene and 2-methylbut-1-en-4-yl ($a\dot{C}_5H_9$-d) radical, Figure 14, was estimated as the addition of $a\dot{C}_5H_9$-d radical to ethylene with a rate constant expression of $1.32 \times 10^4T^{2.48}$ exp(−6130 cal mol^{-1}/*RT*) cm³ mol^{-1} s^{-1}, equivalent to that for ethyl radical addition to a carbon atom in ethylene as recommended by Curran.[65] Furthermore, these rate constants were used for all reactions in which ethyl or a larger radical adds to ethylene, to produce an alkenyl radical.

In the same way, the rate constant of $8.80 \times 10^3T^{2.48}$ exp(−6130 cal mol^{-1}/*RT*) cm³ mol^{-1} s^{-1}, proposed by Curran for ethyl radical addition to an external doubly bound carbon in propene producing an alkenyl radical, was used for all additions

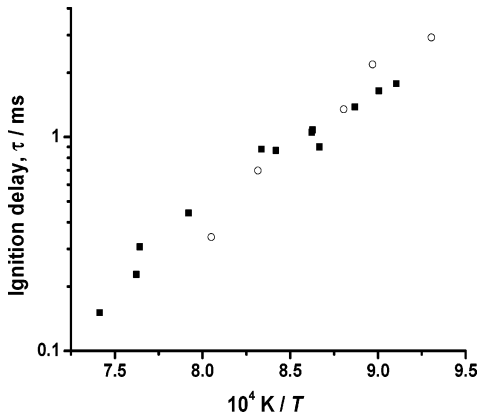

Figure 6. Ignition delay times as a function of inverse temperature at 0.099% MCH/Ar, $\phi = 0.105$, and $p_5 = 1.02$ atm: (■) this study; (○) Hawthorn and Nixon.[40]

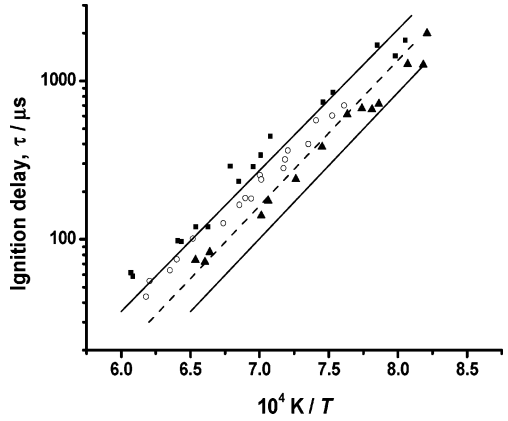

Figure 7. Ignition delay times for a 1.0% MCH in Ar mixture, $\phi = 1.0$ at (■) 1.0 atm, (○) 2.0 atm, and (▲) 4.0 atm. Symbols are experimental results; lines are model predictions. The dashed line corresponds to open symbols.

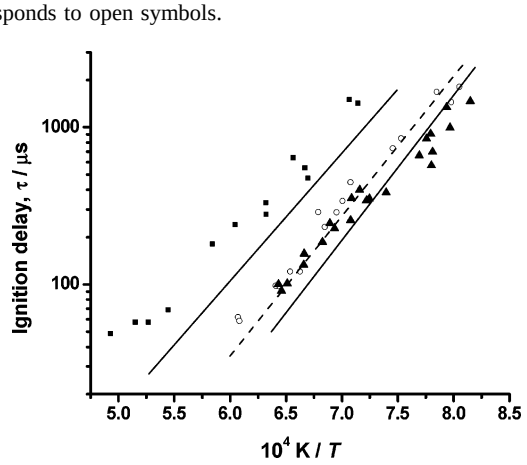

Figure 8. Ignition delay times for MCH in Ar mixtures at 1 atm: (■) $\phi = 2.0$ (1.0% MCH, 5.25% O_2); (○) $\phi = 1.0$ (1.0% MCH, 10.5% O_2); (▲) $\phi = 0.5$ (0.5% MCH, 10.5% O_2). Symbols are experimental results; lines are model predictions.

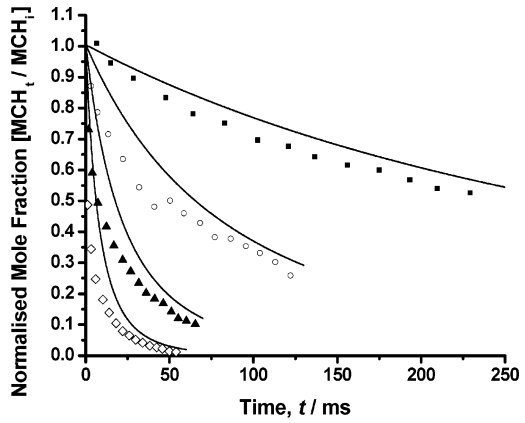

Figure 9. MCH profiles versus time in a flow reactor near-pyrolysis[39] at 1664 ppm MCH, 180 ppm O_2, and 1 atm: (■) 1058 K; (○) 1108 K; (▲) 1154 K; (◇) 1192 K. Symbols are experimental results, lines are model predictions.

of ethyl or larger radicals, to the external doubly bonded carbon in propene or larger alkenes, for example:

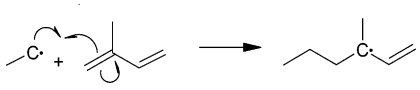

$\dot{C}_2H_5$ adding to isoprene (iC_5H_8) to form 3-methylhex-1-en-3-yl ($g\dot{C}_7H_{13}$-i), Figure 16. The rate constant of $1.76 \times 10^4 T^{2.48}$ exp(−6130 cal mol^{-1}/RT) cm^3 mol^{-1} s^{-1}, recommended by Curran for methyl addition to ethylene, was used for methyl addition to a terminal carbon atom in buta-1,3-diene, for example, methyl addition to buta-1,3-diene forming the pent-1-en-3-yl ($1\dot{C}_5H_9$-3) radical.

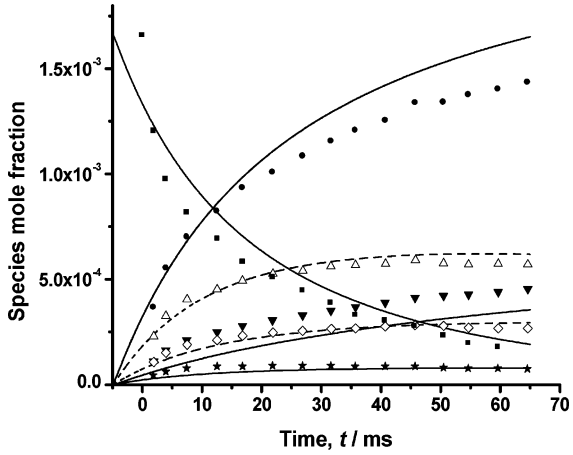

Figure 10. Species profiles versus time in a flow reactor near-pyrolysis[39] at 1664 ppm MCH, 180 ppm O_2, 1155 K, and 1 atm: (■) MCH; (●) C_2H_4; (△) $1,3C_4H_6$; (▼) CH_4; (◇) C_3H_6; (★) iC_5H_8. Symbols are experimental results; lines are model predictions. The dashed line corresponds to open symbols. Time shift = −0.005 s.

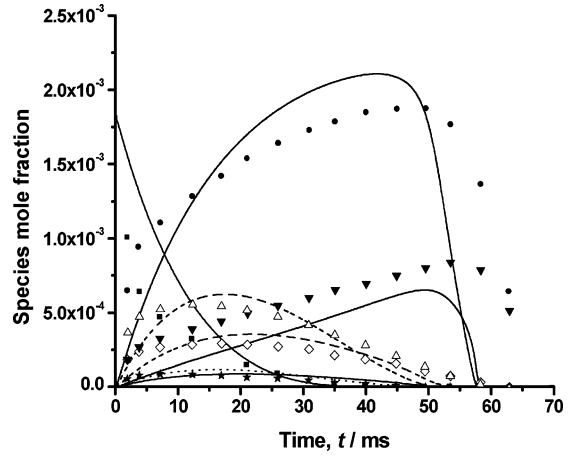

Figure 11. Species profiles versus time in a flow reactor oxidation[39] at 1815 ppm MCH, $\phi = 1.3$, 1160 K, and 1 atm: (■) MCH; (●) C_2H_4; (△) $1,3C_4H_6$; (▼) CH_4; (◇) C_3H_6; (★) iC_5H_8. Symbols are experimental results; lines are model predictions. The dashed line corresponds to open symbols. The dotted line corresponds to penta-1,3-diene simulation, for which no experimental data were available.

With the same assumptions, the rate constant expression of $1.89 \times 10^3 T^{2.67}$ exp(−6850 cal mol^{-1}/RT) cm^3 mol^{-1} s^{-1} recommended by Curran for methyl addition to the internal doubly bound carbon in propene was also used for methyl addition to an equivalent carbon in larger radicals, for example, methyl addition to cyclohexene forming 1-methylcyclohex-2-yl (MCH-R2) radical, Figure 16:

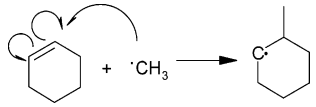

Similarly, the rate constant of $9.45 \times 10^2 T^{2.67}$ exp(−6850 cal mol^{-1}/RT) cm^3 mol^{-1} s^{-1}, for ethyl radical addition to the internal doubly bound carbon atom in propene, was used in all

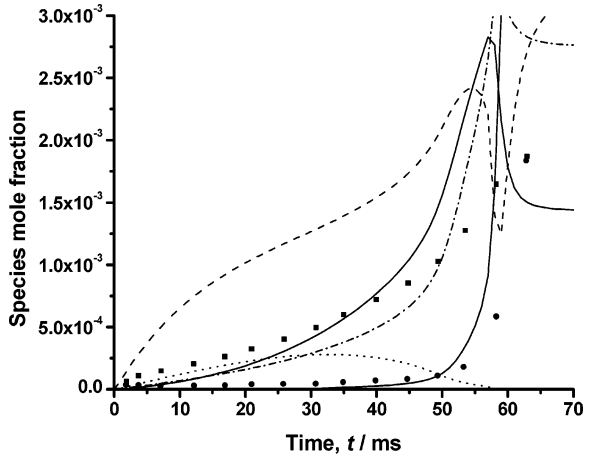

Figure 12. Species profiles versus time in a flow reactor oxidation[39] at 1815 ppm MCH, $\phi = 1.3$, 1160 K, and 1 atm; (■) CO × 0.3; (●) CO_2 × 0.6. Lines: solid = CO × 0.3 and CO_2 × 0.6, dash = H_2, dash dot = H_2O × 0.3, dot = CH_2O. Symbols are experimental results; lines are model predictions.

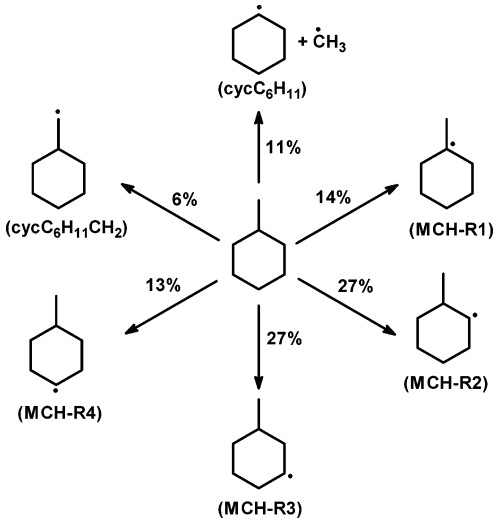

Figure 13. Flux analysis for MCH consumption at 1815 ppm MCH, $\phi = 1.3$, 1160 K, and 1 atm, at 10% consumption.

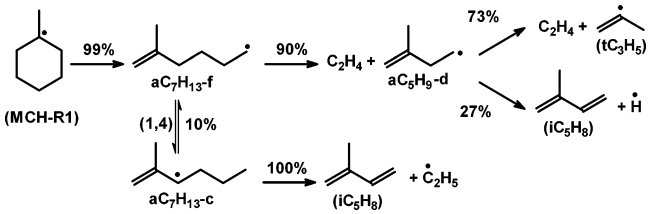

Figure 14. MCH-R1 decomposition. Conditions as per Figure 13.

instances where ethyl or a larger radical added to an internal doubly bound carbon atom in an alkene, for example:

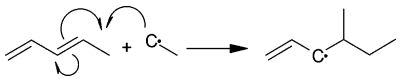

ethyl addition to penta-1,3-diene ($1,3C_5H_8$) forming 4-methyl-hex-1-en-3-yl (kC_7H_{13}-j) radical, Figure 17.

Alkyl Radical Isomerization. The rate constants used for radical isomerization in this study are consistent with those recommended by Matheu et al.,[66] who presented rate constants

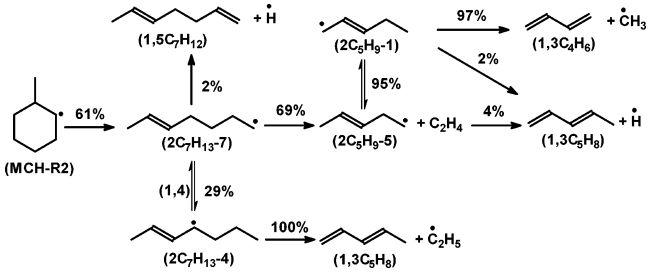

Figure 15. MCH-R2 decomposition. Conditions as per Figure 13.

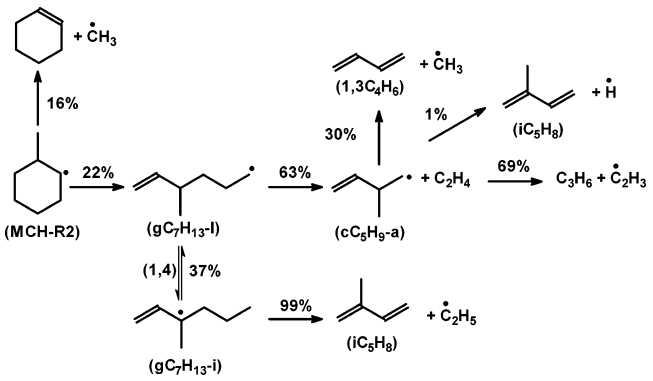

Figure 16. MCH-R2 decomposition. Conditions as per Figure 13.

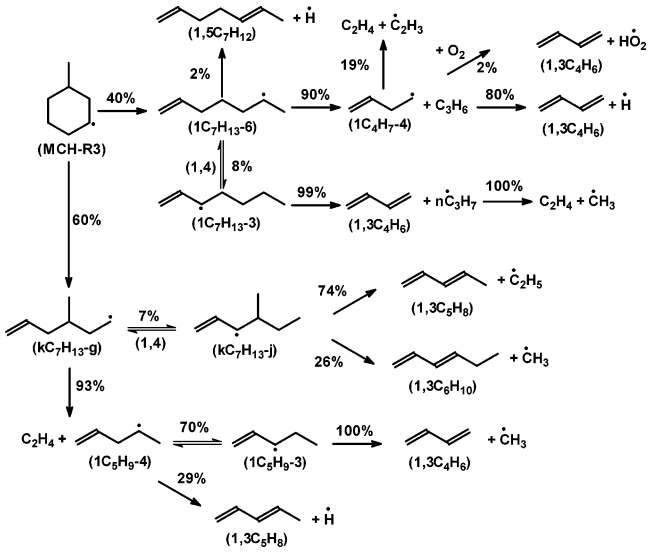

Figure 17. MCH-R3 decomposition. Conditions as per Figure 13.

for these reactions derived from the results of high level (B3LYP-ccpVDZ) quantum calculations by Sumanthi. The frequency (*A*-factor) and temperature dependent (T^n) terms associated with all 1,2 H-shifts are equivalent, with the activation energy of each reaction being dependent on the type (primary, secondary, tertiary, or allylic) of both the initial and final position of the H atom undergoing isomerization. Frequency factors and temperature-dependent terms are also identical for all 1,3 H-shifts and for all 1,4 H-shifts, with the exception of 1,4 primary radical isomerization forming an allylic radical which has unique values. These values have been adopted in the current study and are provided in Table 7.[11]

Matheu defines a "p → s" H-shift as a H-shift within a primary alkyl radical leading to the formation of a secondary alkyl radical and uses the same principle when naming all other H-shifts. However, in this study the type of H atom was used to describe the H-shift. Thus, a H-shift in which the H atom

TABLE 7: Isomerization Reactions; s/cal/mol Units

	A	*n*	E_A
1,2 H-Shifts			
allylic s → s	3.56E+10	0.88	31 500
1,4 H-Shifts			
allylic s → p	3.67E+12	−0.67	15 300
allylic t → p	3.67E+12	−0.67	13 000
allylic s → s	3.67E+12	−0.67	17 900
1,5 H-Shifts			
s → p	3.67E+12	−0.67	12 800
t → p	3.67E+12	−0.67	10 500
s → s	3.67E+12	−0.67	15 300
1,5 H-shifts Forming Allylic Radicals			
allylic s[a] → p	2.80E+10	0.00	7 500
allylic p[b] → p	3.67E+12	−0.60	10 000
1,7 H-Shifts			
hept-2-ene-7-yl → hept-2-ene-1-yl	2.80E+10	0.00	31 640
hept-1,6-diyl → hept-1-ene	2.80E+10	0.00	25 800

[a] An allylic structure is created outside the ring structure in the transition state. [b] A double bond is created inside the ring structure in the transition state.

TABLE 8: E_A (cal mol^{-1}) Calculations for 1,4 and 1,5 H-Shifts[a]

isomerization	type of H-atom	E_A	ΔE_A
	1,4 H-Shifts		
1,4	s → p	20 600	
1,4	t → p	18 300	−2300
1,4	allylic s → p	15 300	
1,4	**allylic t → p**	**13 000**	**−2300**
1,4	s → p	20 600	
1,4	s → s	23 500	+2900
1,4	t → p	18 300	
1,4	t → s	20 600	+2300
1,4	allylic s → p	15 300	
1,4	**allylic s → s**	**17 900**	**+2600[b]**
	1,5 H-Shifts		
1,4	p → p	23 100	
1,4	s → p	20 600	−2500
1,5	p → p	15 300	
1,5	**s → p**	**12 800**	**−2500**
1,4	p → p	23 100	
1,4	t → p	18 300	−4800
1,5	p → p	15 300	
1,5	**t → p**	**10 500**	**−4800**
1,3	p → p	38 800	
1,3	s → s	38 200	−600
1,4	p → p	23 100	
1,4	s → s	23 500	+400
1,5	p → p	15 300	
1,5	**s → s**	**15 300**	**+0[c]**
	1,5 H-Shifts Forming Allylic Radicals		
1,4	p → p	23 100	
1,4	allylic s → p	15 300	−7800
1,5	p → p	15 300	
1,5	**allylic s → p**	**7500**	**−7800**
1,4	s → p	20 600	
1,4	allylic s → p	15 300	−5300
1,5	p → p	15 300	
1,5	**allylic p → p**	**10 000**	**−5300**

[a] Bold entries have E_A values derived from those recommended by Matheu.[66] [b] +2600 = average ΔE_A for two previous entries, that is, +2900 and 2300. [c] 0 ≈ average ΔE_A for two previous entries.

moves from a primary carbon atom to a secondary carbon atom is defined as a "p → s" H-shift.

Further analysis of the rate constants recommended by Matheu et al.[66] indicated that there were general trends in activation energy for the isomerization of primary, secondary, tertiary, and allylic H atoms. The trends observed for 1,2, 1,3, and 1,4 H-shifts were used to extrapolate Matheu's work and estimate activation energies for isomerization reactions that occurred during MCH oxidation but were not previously specified. Table 8 shows the calculated E_A values (in bold), together with the E_A values that were defined by Matheu for relevant reactions. A complete list of rate constants used for isomerization reactions is provided in Table 7.

The rate expression of $3.56 \times 10^{10}T^{0.88}$ exp(−31500 cal mol^{-1}/*RT*) cm^3 mol^{-1} s^{-1} for a 1,2 allylic s → s H-shift, for example,

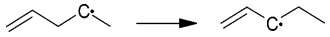

pent-1-en-4-yl ($1\dot{C}_5H_9$-4) forming pent-1-en-3-yl ($1\dot{C}_5H_9$-3), was taken directly from Matheu and used in this study, Table 7.

The rate expression of $3.67 \times 10^{12}T^{-0.6}$ exp(−15300 cal mol^{-1}/*RT*) cm^3 mol^{-1} s^{-1} was used by Matheu for 1,4 H-shifts in which a primary radical isomerized to form a secondary allylic radical. In this study these *A* and T^n terms were used for all 1,4 H-shifts, Table 7. An E_A of 15.3 kcal mol^{-1} was used for 1,4 allylic s → p H-shifts, for example:

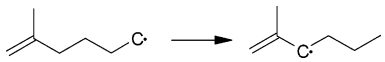

2-methylhex-1-en-6-yl ($a\dot{C}_7H_{13}$-f) radical forming 2-methylhex-1-en-3-yl ($a\dot{C}_7H_{13}$-c) radical, Figure 14.

The activation energy was decreased by 2.3 kcal mol^{-1} to 13.0 kcal mol^{-1} for 1,4 allylic t → p H-shifts), Table 7, for example:

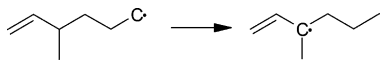

3-methylhex-1-en-6-yl ($g\dot{C}_7H_{13}$-l) radical forming 3-methylhex-1-en-3-yl ($g\dot{C}_7H_{13}$-i) radical, Figure 16. This corresponds to the difference in activation energy between an s → p and a t → p H-shift, Table 8. For 1,4 allylic s → s H-shifts, for example,

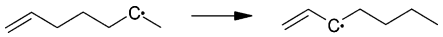

hept-1-en-6-yl ($1\dot{C}_7H_{13}$-6) radical forming hept-1-en-3-yl ($1\dot{C}_7H_{13}$-3) radical, Figure 17, the activation energy was instead increased by 2.6 kcal mol^{-1} to 17.9 kcal mol^{-1}, Table 7. This change in energy corresponds to the average difference between 1,4 s → p and s → s, and t → p and t → s H-shifts, Table 8.

The rate constant expression of $3.67 \times 10^{12}T^{-0.6}$ exp(−15300 cal mol^{-1}/*RT*) cm^3 mol^{-1} s^{-1} is recommended by Matheu for 1,5 H-shifts in which a primary radical isomerizes to form a primary radical. These *A*-factor and T^n values were used in this study for all 1,5 H-shifts that did not result in the formation of an allylic radical, Table 7. As before the E_A value was adjusted for individual reactions. For instance, when a primary radical site on a diradical isomerized through a 1,5 H-shift to a secondary position forming an alkene (that is, s → p H-shifts), for example,

hept-1,6-diyl ($\dot{C}_7H_{14}$-1,6) forming hept-2-ene ($2C_7H_{14}$), the activation energy was decreased by 2.5 kcal mol^{-1} to 12.8 kcal mol^{-1}, which corresponds to the difference in energy between a p → p and s → p 1,4 H-shifts, Table 8.

In the case of a primary radical site on a diradical isomerizing to a tertiary site forming an alkene (that is, a t → p 1,5 H-shift), for example,

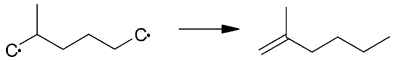

2-methylhex-1,6-diyl ($\dot{C}_7H_{14}$-a,f) forming 2-methylhex-1-ene (aC_7H_{14}), the activation energy was decreased by 4.8 kcal mol^{-1} to 10.5 kcal mol^{-1}, which is equal to the difference in energy between 1,4 p → p and t → p H-shifts, Table 8.

For reactions in which a secondary radical site on a diradical isomerized by a 1,5 H-shift to a secondary site forming an alkene (that is, a s → s H-shift), for example,

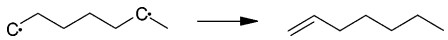

hept-1,6-diyl ($\dot{C}_7H_{14}$-1,6) forming hept-1-ene ($1C_7H_{14}$), no changes were made to the activation energy due to the fact that the rate expressions recommended by Matheu have very similar activation energies for both 1,3 and 1,4 p → p and s → s H-shifts, Table 8.

In cases where allylic radicals were formed from 1,5 H-shifts different rules were used to estimate rate constants for the reactions. When 1,5 allylic s → p H-shifts involved the formation of an allylic radical outside the ring structure in the transition state, for example,

hept-1-en-7-yl ($1\dot{C}_7H_{13}$-7) forming hept-1-en-3-yl ($1\dot{C}_7H_{13}$-3), the rate expression was estimated using the *A*-factor and T^n value recommended by Matheu for 1,6 H-shifts, Table 7. This compensates for the loss of an extra internal rotor in the molecule as an allylic radical is formed in a position β to the 1,5 shift. The activation energy was taken as 7.50 kcal mol^{-1}, which is the activation energy for p → p 1,5 H-shifts (15.3 kcal mol^{-1}) minus the difference in energy between 1,4 p → p and allylic s → p (7.8 kcal mol^{-1}), Table 8. This yielded a rate constant of 2.8×10^{10} exp(−7500/*RT*) cm^3 mol^{-1} s^{-1}, Table 7.

For 1,5 allyl p → p H-shifts, where the double bond is present in the ring structure of the transition state, that is, in the case of

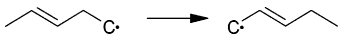

pent-2-en-5-yl ($2\dot{C}_5H_9$-5) forming pent-2-en-1-yl ($2\dot{C}_5H_9$-1), the *A*-factor and T^n value recommended by Matheu for 1,4 H-shifts forming a secondary allylic from a primary radical were used, due to one less rotor being lost in the transition state, Table 7. The activation energy for 1,5 p → p H-shifts was decreased by 5.3 kcal mol^{-1}, which corresponds to the difference in activation energy between s → p (20.6 kcal mol^{-1}) and allylic s → p (15.3 kcal mol^{-1}) 1,4 H-shifts, Table 8. This resulted in a rate constant of $3.67 \times 10^{12}T^{-0.6}$ exp(−10000 cal mol^{-1}/*RT*) cm^3 mol^{-1} s^{-1}, Table 7.

In the case of

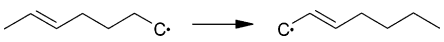

hept-2-en-7-yl ($2\dot{C}_7H_{13}$-7) → hept-2-en-1-yl ($2\dot{C}_7H_{13}$-1), a 1,7 H-shift occurred and a double bond was present in the seven-membered cyclic transition state. For this isomerization the *A*-factor and T^n value recommended by Matheu for 1,6 H-shifts were used due to one less rotor being lost in transition state formation, Table 7. The activation energy was estimated using the Evans−Polanyi rule devised by Matheu with the ring strain being estimated as 11.0 kcal mol^{-1} (10.0 kcal mol^{-1} for an eight-membered cyclic transition state[67] plus 1.0 kcal mol^{-1} to account for the extra strain caused by the double bond in the cyclic transition state[68]). This leads to a rate expression of 2.8×10^{10} exp(−31640 cal mol^{-1}/*RT*) cm^3 mol^{-1} s^{-1}, Table 7.

For 1,7 H-shifts from a primary to primary position, which resulted in a double bond being formed inside the ring structure of the transition state, that is

hept-1,6-diyl ($\dot{C}_7H_{14}$-1,6) forming hept-1-ene ($1C_7H_{14}$), the *A*-factor and T^n value recommended by Matheu for 1,6 H-shifts were used. The activation energy was estimated to be 25.8 kcal mol^{-1}. This value was calculated by increasing the ring strain of cyclooctane by the average difference between the ring strain of four-, five-, and six-membered cyclic hydrocarbons and the activation energy for primary to primary H-shifts that proceed through the corresponding four-, five-, and six-membered transition states, Table 11. As before, 1.0 kcal mol^{-1} was added to compensate for the extra ring strain incurred by the formation of a double bond inside the ring structure of the transition state. This resulted in a rate constant of 2.8×10^{10} exp(−25800 cal mol^{-1}/*RT*) cm^3 mol^{-1} s^{-1}, Table 7.

Other Alkene/Alkenyl Radical Decompositions. The rate constant for cyclohexa-1,3-diene decomposition forming benzene and molecular hydrogen was estimated to be $2.36 \times 10^{19}T^{-1.38}$ exp(−67530 cal mol^{-1}/*RT*) cm^3 mol^{-1} s^{-1} by creating a best fit though the data provided for this reaction by Orchard et al.[69] and Alfassi et al.[70] A rate constant of 5.01×10^{15} exp(−72600 cal mol^{-1}/*RT*) cm^3 mol^{-1} s^{-1} was reported by Dean[71] for cyclohexa-1,3-diene decomposition forming cyclohexa-2,4-dien-1-yl and a hydrogen atom and was used in this study.

The cyclohexa-2,4-dien-1-yl radical (1,3CYCHEX-5) can decompose via two pathways:

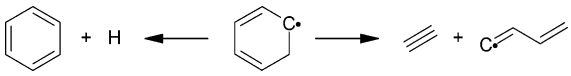

For the first reaction, which produces C_2H_2 and $n\dot{C}_4H_5$ radicals, the rate constant of $2.51 \times 10^{14}T^{0.7}$ exp(−41830 cal mol^{-1}/*RT*) cm^3 mol^{-1} s^{-1} recommended by Weissman et al.[72] was used. The rate constant of $4.80 \times 10^{25}T^{-3.5}$ exp(−33480 cal mol^{-1}/*RT*) cm^3 mol^{-1} s^{-1} for the decomposition producing benzene and a hydrogen atom was estimated by generating a best fit of the data provided by Dean[71] and Nicovich et al.[73] for this reaction.

In the same way the rate constant for cyclohexene decomposition to give buta-1,3-diene and ethylene was estimated to be $3.64 \times 10^{62}T^{-13.8}$ exp(−92030 cal mol^{-1}/*RT*) cm^3 mol^{-1} s^{-1} by creating a best fit of the data provided for this reaction using the studies of Lewis et al.,[74] Hidaka et al.,[75] Skinner et al.,[76] Newman et al.,[77] Barnard et al.,[78] and Tsang.[79,80]

Ring Opening Reactions. The ring opening reactions were written in the reverse intramolecular alkenyl radical ring closure direction and the rate constants were estimated in this direction. Rate constants for ring closure leading to the formation of cyclic radical species, for example:

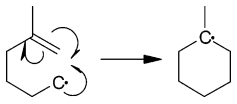

2-methylhex-1-en-6-yl ($a\dot{C}_7H_{13}$-f) forming 1-methylcyclohex-1-yl (MCH-R1), Figure 14, were derived from those reported by Matheu et al.,[66] who presented high-pressure-limit rate rules for radical additions and ring opening/closing reactions. Radical addition rules developed by Matheu et al.[66] were taken from

TABLE 9: E_A (cal mol^{-1}) Calculations for Ring Closing Reactions[a]

	E_A	ΔE_A
Intra 1,6 Addition (Endo)		
alkyl addn to terminal C atom of double bond	7800	
alkyl addn to internal C atom of double bond	10 600	+2800
○ 1° Ċ radical addition to external C═C	5900	
○ 1° Ċ radical addition to internal C═C	**8700**	**+2800**
1,4 s → p H-shift	20 600	
1,4 s → s H-shift	23 500	+2900
1,4 t → p H-shift	18 300	
1,4 t → s H-shift	20 600	+2300
○ 1° Ċ radical addition to external C═C	5900	
○ 2° Ċ radical addition to external C═C	**8500**	**+2600[b]**
Intra 1,6 Addition (Exo)		
○ cyclo-propyl (endo) ring opening	21 900	
○ cyclo-propyl (exo) ring opening	7060	divided by 3.1
○ 1° C radical addition to external C═C (endo)	5900	
○ 2° C radical addition to external C═C (exo)	**1903**	**divided by 3.1**

[a] Bold entries have E_A values derived from those recommended by Matheu;[66] all others are taken directly from Matheu. [b] +2600 = average ΔE_A for two previous entries, that is, +2900 and +2300. [c] ○ denotes ring closing/opening reactions.

the work of Curran and co-workers,[54] and in the case of vinyl addition, from Fahr and Stein.[81] Rate rules for cycloalkyl ring closures or openings were taken by Matheu et al. from model reactions listed by Newcomb where available;[82] otherwise, they were estimated using both simple (rigid-rotor harmonic oscillator) transition-state theory (TST) and detailed ab initio calculations. There are two distinct types of ring closure defined by Matheu et al. as "exo" and "endo" ring opening/closure; for "exo" ring closure the radical site is β to the carbon ring (radical addition in the alkenyl radical occurs on the internal doubly bound carbon), and for "endo" ring closure the radical site is on the ring itself (radical addition occurs on the terminal doubly bound carbon).

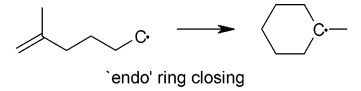

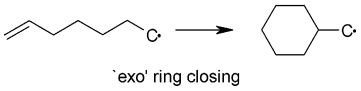

In this study "endo" 1,6 intramolecular ring closures have been treated by taking the rate constant expression of Matheu et al. for primary carbon radical addition to an external doubly bound carbon atom, that is, $1.0 \times 10^8 T^{0.86} \exp(-5900 \text{ cal mol}^{-1}/RT)$ cm^3 mol^{-1} s^{-1}. Though these A-factor and T^n values were used in this study for all "endo" 1,6 intramolecular ring closures, the activation energy, E_A, was altered for individual reactions to allow for (i) increased ring strain, (ii) different radical types, and (iii) the location of the carbon atom to which addition occurred. Alterations to the E_A value were made by analyzing the differences between E_A values presented by Matheu et al. for relevant reactions and changing the E_A value of 5.9 kcal mol^{-1} by the same amount. More detailed explanations are given in the following section. Table 9 shows the calculated E_A values (in bold), along with the E_A values that were defined by Matheu et al. for relevant reactions, with Table 10 listing the A, T^n, and E_A values for each type of ring closing reaction.

The rate constant of $1.0 \times 10^8 T^{0.86} \exp(-5900 \text{ cal mol}^{-1}/RT)$ cm^3 mol^{-1} s^{-1} was used without modification in cases where addition occurred specifically as outlined by Matheu et al., for example, 2-methylhex-1-en-6-yl (aC_7H_{13}-f) forming 1-methylcyclohex-1-yl (MCH-R1) radical, Figure 14 (any effects caused by the methyl group were ignored), Table 10.

TABLE 10: Ring Closing Reactions; s/cal/mol Units

	A	n	E_A
Intra 1,6 Addition (Endo)			
1° Ċ radical addition to external C═C	1.0E+08	0.86	5900
1° Ċ radical addition to internal C═C	1.0E+08	0.86	8700
2° Ċ radical addition to external C═C	1.0E+08	0.86	8500
1° Ċ radical addition to external C═C[a]	1.0E+08	0.86	6900
Intra 1,6 Addition (Exo)			
1° Ċ radical addition to internal C═C	1.0E+08	0.86	1903

[a] A C═C bond is contained in the ring structure of the transition state.

TABLE 11: Differences between Ring Strain and E_A (cal mol^{-1}) for a H-Shift Incorporating an Equivalent Transition State[a]

	ring strain	H-shift	E_A for p → p H-shift	ΔE_A
cyclobutane	26 300	1,3	38 800	12 500
cyclopentane	6500	1,4	23 100	16 600
cyclohexane	0	1,5	15 300	15 300
cycloheptene	**10 000**	**1,7**	**24 800**	**14 800[b]**

[a] Bold entries are calculated values. [b] 14 800 = average difference between E_A and ring strain.

For "endo" 1,6 primary carbon radical addition to an internal doubly bonded carbon, for example,

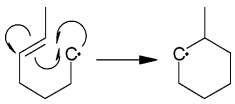

hept-2-en-7-yl (2C_7H_{13}-7) forming 1-methylcyclohex-2-yl (MCH-R2), Figure 15, the activation energy for addition to a terminal doubly bound carbon was increased by 2.80 kcal mol^{-1} to 8.70 kcal mol^{-1}, consistent with the increase in activation energy between alkyl radical addition to the terminal and internal carbon atoms of a double bond as reported by Matheu et al.,[66] Tables 9 and 10.

In the case of "endo" 1,6 secondary carbon radical addition to an external doubly bound carbon, for example,

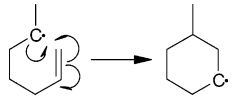

hept-1-en-6-yl (1Ċ$_7H_{13}$-6) forming 1-methylcyclohex-3-yl (MCH-

R3) radical, the activation energy was increased by 2.60 kcal mol^{-1} to 8.50 kcal mol^{-1}, which is the average difference in activation energy between 1,4 s → p and s → s, and t → p and t → s H-shifts, Tables 9 and 10.

For "endo" 1,6 primary carbon radical addition to an external doubly bonded carbon atom when an extra double bond was present in the ring, for example,

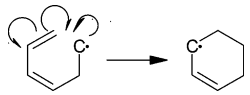

hexa-1,3-dien-6-yl ($1,3\dot{C}_6H_9$-6) forming cyclohex-1-en-3-yl ($cyc\dot{C}_6H_9$-3) radical, 1.0 kcal mol^{-1} was added to the activation energy and a value of 6.9 kcal mol^{-1} was used, Table 10. This corresponds to the difference in ring strain between cyclohexane and cyclohexene[68] and compensates for the extra energy needed for the ring structure to be formed.

For "exo" 1,6 intramolecular cyclo-alkyl ring closing, that is, where the radical site is β to the carbon ring, for example,

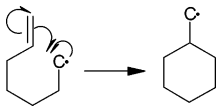

hept-1-en-7-yl ($1\dot{C}_7H_{13}$-7) forming CYCHEXCH2, the same rate constant of $1.0 \times 10^8 T^{0.86} \exp(-5900 \text{ cal mol}^{-1}/RT)$ cm^3 mol^{-1} s^{-1} was used but the activation energy was reduced by a factor of 3.1, yielding a value of 1903 cal mol^{-1}, Tables 9 and 10. This corresponds to the ratio of the activation energies for "endo" and "exo" cyclopropyl ring opening. Although this value is perhaps not entirely suitable, the sensitivity analysis does not highlight the rate of this reaction as being very significant for MCH combustion.

Results and Discussion

Shock Tube Ignition Delays. Shock tube ignition delay times for MCH/O_2/Ar mixtures were measured behind reflected shock waves over the temperature range 1250−2100 K at reflected shock pressures of 1.0, 2.0, and 4.0 atm, and equivalence ratios, ϕ, of 0.5, 1.0, and 2.0, Figures 6−8. Delay times of over 1 ms to fewer than 50 μs were recorded. Shorter delay times were observed, but the corresponding percentage error accounted in some cases for a large portion of the delay. For this reason delay times of less than 50 μs were ignored.

To perform a comparative study, the shock tube experiments of Hawthorn and Nixon[40] were repeated. Although these experiments had been performed behind incident shock waves, their conditions of temperature and pressure were reproduced in the current study to compare the results directly. Figure 6 depicts ignition delay times as a function of inverse temperature at 0.099% MCH/Ar, $\phi = 0.105$, at a pressure of 1.02 atm measured behind the reflected shock in the present study and behind the incident shock by Hawthorn and Nixon. For these experiments, the ignition delay time was defined as the time between the shock arrival at the end wall and the first light emission, as measured from the end wall. For experiments in this study, the same end-on detection diagnostic was used (with the filter removed). The data generated in the current study and those recorded by Hawthorn and Nixon are in very good agreement, although it could be argued that the data of Hawthorn and Nixon shows a slightly higher activation energy relative to that measured in the current study.

The ignition delay times obtained for a 1.0% MCH/10.5% O_2 stoichiometric ($\phi = 1.0$) mixture, over the temperature range 1300−2200 K, at pressures of 1.0, 2.0, and 4.0 atm, are shown in Figure 7, together with model predictions. The ignition delay times decrease as the reflected shock pressure is increased progressively from 1.0 to 2.0 and then 4.0 atm, in agreement with most studies carried out to date[45] on hydrocarbons. The ignition delay times simulated using the MCH mechanism, in conjunction with the Chemkin III suite of programs, are slightly faster than those measured experimentally but they accurately capture the pressure dependence.

Ignition delay times for different MCH/O_2 mixtures measured at atmospheric pressure are shown in Figure 8, together with simulated ignition delay times. Increasing the oxygen concentration from 5.25% ($\phi = 2.0$) to 10.50% ($\phi = 1.0$), with a constant MCH concentration of 1.0%, led to a significant reduction in delay times. This negative power dependence of oxygen is in accordance with previous work.[45] Conversely, as the MCH concentration was increased from 0.5% ($\phi = 0.5$) to 1.0% ($\phi = 1.0$), with the O_2 concentration constant at 10.5%, the ignition delay times increased but the magnitude of this effect was much less pronounced than in the case of oxygen. This observation is also in agreement with previous studies of hydrocarbons. The concentration of argon in all three mixtures was essentially constant and so did not influence the delay times. Model-predicted ignition delay times are slightly faster than those measured but do accurately capture the influence of fuel and oxygen concentration.

Modeling of Turbulent Flow Reactor. The MCH mechanism was used to simulate the species profiles measured for MCH near-pyrolysis and oxidation in a turbulent flow reactor by Zeppieri et al.[39] MCH pyrolysis decay profiles were determined as functions of time at 1664 ppm MCH, 180 ppm O_2, 1 atm, and at four temperatures (1058, 1108, 1154, and 1192 K). The detailed chemical kinetic mechanism was used to simulate these data and a comparison of the experiment and model predictions are provided in Figure 9. Overall, the model captures the experimental trends of fuel consumption in that, as the reactor temperature increases, the fuel decay time decreases and the profiles become much steeper.

The experiments also produced species profiles versus time for MCH near-pyrolysis at 1664 ppm MCH, 180 ppm O_2, 1155 K, 1 atm, Figure 10. In addition, species profiles were also recorded for MCH oxidation at 1815 ppm MCH, $\phi = 1.3$, 1160 K, 1 atm, Figure 11. Major products, for both oxidation and pyrolysis, included methane (CH_4), ethylene (C_2H_4), propene (C_3H_6), buta-1,3-diene ($1,3C_4H_6$), and isoprene (iC_5H_8). Aromatic and cyclic hydrocarbon species were among the minor products recorded, as were ethane and some unsaturated C_2, C_3, and C_4 hydrocarbons. The detailed chemical kinetic mechanism created in this study was used to simulate both the pyrolysis and oxidation experiments, Figures 10 and 11.

All simulated species profiles for the pyrolysis experiments were time-shifted by −5 ms relative to the experiments to allow for the experimental uncertainties of the time−temperature history of the in-flowing reactants. Time-shifting the simulated pyrolysis data by this amount led to the best overall agreement between the experimental and predicted fuel-consumption profiles, Figure 10. The MCH profile does not decrease as rapidly as the experimental data between 5 and 25 ms, but the overall agreement is quite good. In general, the shape and magnitude of the major species profiles are in good agreement with the experimental data but methane production is under-predicted by ≈20%.

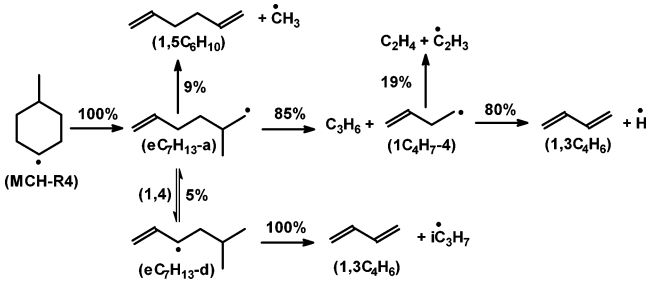

Figure 18. MCH-R4 decomposition. Conditions as per Figure 13.

In the oxidative case, for which no time-shifting was necessary, the MCH profile does not fall off as rapidly as the experimental data between 0 and 25 ms, Figure 11. Again, most of the major species profiles are in generally good agreement. Species production does not occur as rapidly as the experimental data suggest between 0 and 5 ms, and the model also predicts that all species profiles will have dropped to near zero at ≈58 ms whereas the experimental data drop to near zero at ≈63 ms. Again, methane is underpredicted by ≈20%.

Some species predicted by the model were not observed under the oxidation experimental conditions. Hydrogen, water, and formaldehyde were predicted in relatively large quantities, and penta-1,3-diene was also predicted, albeit on a much smaller scale, Figures 11 and 12. The analytical techniques (MS and GC-MS) employed may not have been entirely suitable for the detection and quantification of hydrogen, CH_2O, and H_2O.[83]

Rate of Production Analysis. A rate of production analysis was performed using Chemkin in the case of the MCH oxidation in the flow reactor, at 1815 ppm MCH, 14 660 ppm O_2 (ϕ = 1.3), 1160 K, 1 atm, at a time corresponding to 10% MCH consumption. This analysis revealed that oxidation occurs by H-atom abstraction from the fuel, Figure 13. Hydrogen abstraction by molecular oxygen, Ḣ and Ȯ atoms, and $\dot{C}H_3$, $H\dot{O}_2$, ȮH, and $CH_3\dot{O}$ radicals, occurs at primary, secondary, and tertiary (1°, 2°, and 3°) sites, leading to the formation of five different methylcyclohexyl radicals, Figure 13. The rates for abstraction by different radical species were assumed to be equivalent to H-atom abstraction rates from similar sites in other alkane molecules and the rate constants used are shown in Table 5.

Figure 13 shows the relative importance of the abstraction pathways. Flux analysis shows that secondary H-atom abstraction dominates, leading preferentially to the formation of MCH-R2, MCH-R3, and MCH-R4. MCH-R2 and MCH-R3 are formed in equal concentrations (≈27%) whereas MCH-R4 accounts for approximately 13% of the fuel. This is due to the degeneracy of the system, as there are four equivalent hydrogen atoms available to form MCH-R2 and MCH-R3 but there are only two hydrogen atoms in the case of MCH-R4. Tertiary hydrogen atom abstraction leads to the formation of MCH-R1 (≈14%) whereas primary hydrogen atom abstraction produces the cyclohexyl−methylene radical (≈6%). Finally, the unimolecular decomposition of MCH producing a cyclohexyl and a methyl radical accounts for approximately 11% of MCH.

The decomposition of the methylcylohexyl radicals MCH-R1, MCH-R3, and MCH-R4 are detailed in Figures 14, 17, and 18, respectively. The two ring opening steps and the β-scission step, by which MCH-R2 decomposes are illustrated in Figures 15 and 16. MCH-R1, which accounts for 14% of the fuel, undergoes a ring opening reaction to form 2-methylhex-1-en-6-yl ($a\dot{C}_7H_{13}$-f), Figure 14. This in turn undergoes β-scission (90%) forming 2-methylbut-1-en-4-yl ($a\dot{C}_5H_9$-d) and ethylene. The $a\dot{C}_5H_9$-d forms tC_3H_5 plus ethylene by β-scission (73%) and isoprene ($i\dot{C}_5H_8$) plus H-atom (27%). The other 10% of $a\dot{C}_7H_{13}$-f isomerizes to form 2-methylhex-1-en-3-yl ($a\dot{C}_7H_{13}$-c), which then forms isoprene plus $\dot{C}_2H_5$.

MCH-R2 decomposes via three different pathways, Figures 15 and 16:

1. 61% forms hept-2-en-7-yl ($2\dot{C}_7H_{13}$-7), which proceeds via β-scission (69%) to yield pent-2-en-5-yl ($2\dot{C}_5H_9$-5) plus ethylene. $2\dot{C}_5H_9$-5 then isomerizes to yield pent-2-en-1-yl ($2\dot{C}_5H_9$-1) (95%), which in turn forms butadiene plus methyl radical (97%). Another 29% of $2\dot{C}_7H_{13}$-7 isomerizes to form hept-2-en-4-yl ($2\dot{C}_7H_{13}$-4), which then yields penta-1,3-diene ($1,3C_5H_8$) plus $\dot{C}_2H_5$ radical, Figure 15.
2. 16% of MCH-R2 undergoes β-scission, producing cyclohexene plus methyl radical, Figure 16.
3. 22% undergoes ring opening, producing 3-methylhex-1-en-6-yl ($g\dot{C}_7H_{13}$-l). $g\dot{C}_7H_{13}$-l then decomposes via two different pathways. 37% undergoes isomerization to form 3-methylhex-1-en-3-yl ($g\dot{C}_7H_{13}$-i), which then yields isoprene plus $\dot{C}_2H_5$. The other 63% of $g\dot{C}_7H_{13}$-l undergoes β-scission to give 2-methylbut-3-en-1-yl ($c\dot{C}_5H_9$-a) plus ethylene. $c\dot{C}_5H_9$-a yields propene plus $\dot{C}_2H_3$ (69%) and butadiene plus methyl radical (30%), Figure 16.

The decomposition of MCH-R3 occurs via two major ring opening pathways, Figure 17. In the first pathway, 60% forms 3-methylhex-5-en-1-yl ($k\dot{C}_7H_{13}$-g). This primarily (93%) undergoes β-scission to form pent-1-en-4-yl ($1\dot{C}_5H_9$-4) plus ethylene. The $1\dot{C}_5H_9$-4 species then either isomerizes (70%) to form pent-1-en-3-yl ($1\dot{C}_5H_9$-3), which then produces butadiene plus methyl, or forms penta-1,3-diene ($1,3C_5H_8$) plus H-atom (29%). In the second pathway, MCH-R3 forms hept-1-en-6-yl ($1\dot{C}_7H_{13}$-6) (40%) via a different ring opening step. The $1\dot{C}_7H_{13}$-6 then decomposes via β-scission (90%) to form propene plus but-1-en-4-yl ($1\dot{C}_4H_7$-4), which in turns yields butadiene plus H-atom (80%). Another 8% of $1\dot{C}_7H_{13}$-6 isomerizes to form hept-1-en-3-yl ($1\dot{C}_7H_{13}$-3), which gives butadiene plus $n\dot{C}_3H_7$. The $n\dot{C}_3H_7$ radical then forms ethylene plus methyl radical.

MCH-R4 decomposes via one ring opening step to form 2-methylhex-5-en-1-yl ($e\dot{C}_7H_{13}$-a), Figure 18. The majority (85%) of this undergoes β-scission to form propene plus but-1-en-4-yl ($1\dot{C}_4H_7$-4), which in turn forms butadiene plus H-atom (80%).

Chemical Kinetic Mechanism: Sensitivity Analysis. The addition of the species and reactions necessary for MCH oxidation to the original mechanism of Laskin et al. for buta-1,3-diene oxidation, resulted in a chemical kinetic mechanism containing 190 species and 904 reversible reactions. To carry out the sensitivity analysis, the *A*-factor of a reaction was increased by a factor of 2 and the altered mechanism was used to simulate MCH oxidation under particular conditions. Two sensitivity analyses were performed, one showing sensitivity to ignition delay times and the second to fuel consumption in the flow reactor.

Sensitivity analysis of shock tube ignition delay times was carried out using a 1% MCH, 10.5% O_2 in 88.5% Ar mixture, at a reflected shock pressure of 1.0 atm at temperatures of 1250 and 1667 K. For each reaction, the percentage difference in ignition delay time for the altered and unaltered mechanisms was measured. A negative sensitivity value indicates a decrease in the ignition delay time and thus an increase in overall reactivity. Figure 19 contains the coefficients for reactions contained in the Laskin et al.[52] buta-1,3-diene and the Ó Conaire[53] H_2/O_2 submechanisms. Reactions with a sensitivity coefficient of less than 3% were excluded. Figure 20 depicts sensitivity coefficients for all reactions that were added in this

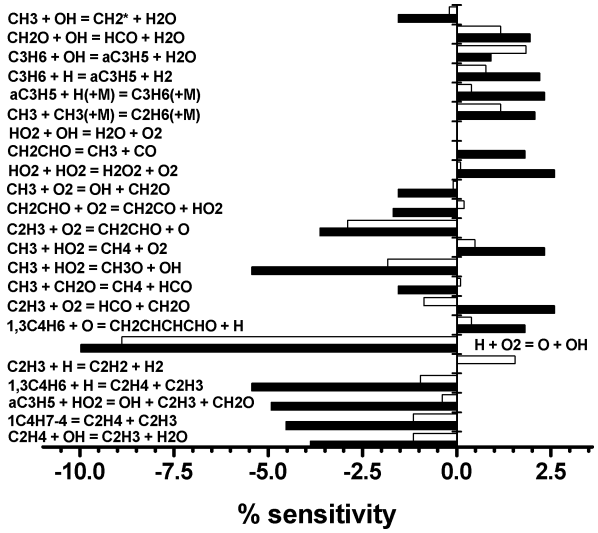

Figure 19. Sensitivity analysis for shock tube ignition delay times at 1.0% MCH in Ar mixture, $\phi = 1.0$, and 1.0 atm: (■) 1250 K; (□) 1667 K.

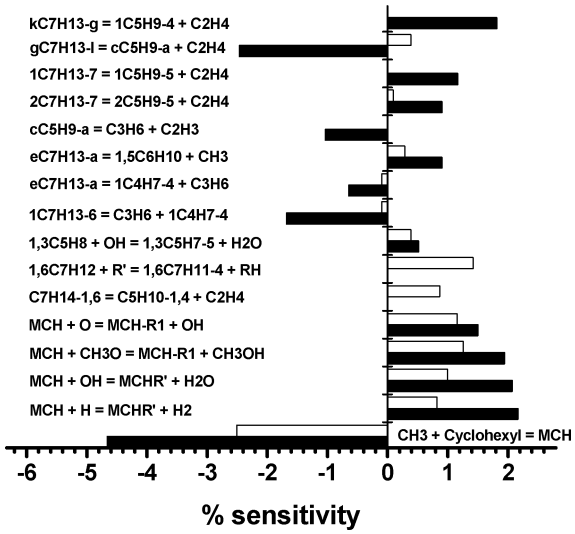

Figure 20. Sensitivity analysis for shock tube ignition delay times at 1.0% MCH in Ar mixture, $\phi = 1.0$, and 1.0 atm; (■) 1250 K; (□) 1667 K. (MCHR′ = all methylcyclohexyl radicals.)

study for the C_5, C_6, and C_7 submechanisms. In this case reactions with sensitivity coefficients of less than 1% were excluded.

The shock tube sensitivity analysis highlighted the large negative sensitivity of the decomposition reaction of MCH to cyclohexyl and a methyl radical; that is, increasing the *A*-factor of this reaction caused the ignition delay times to decrease significantly at both 1250 and 1667 K. To understand this observation a flux analysis was carried out at 1250 K at a time of 107 μs, that is, the time at which 10% fuel had been consumed. This showed that 9% of MCH consumed decomposes to give cyclohexyl and a methyl radical:

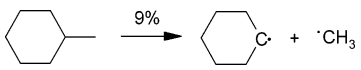

The cyclohexyl radical then forms hex-1-en-6-yl ($1C_6H_{11}$-6):

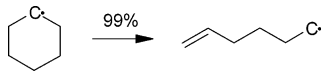

which in turn decomposes to give 90% but-1-en-4-yl ($1\dot{C}_4H_7$-4) plus ethene (C_2H_4):

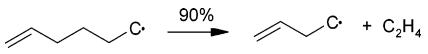

78% of but-1-en-4-yl produces buta-1,3-diene ($1,3C_4H_6$) and a H-atom (73%) by C−H bond homolysis, or $H\dot{O}_2$ by reaction with O_2 (5%):

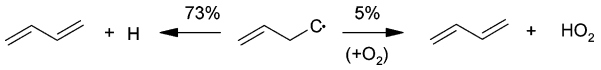

The other 21% of the but-1-en-4-yl undergoes β-scission to produce ethylene and vinyl ($\dot{C}_2H_3$) radical:

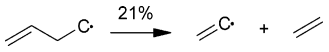

It should also be noted that, in addition to MCH decomposition forming cyclohexyl and a methyl radical, other reactions that favored the formation of $\dot{C}_2H_3$ also have negative sensitivity values, Figure 19. These included

$$C_2H_4 + \dot{O}H \rightarrow \dot{C}_2H_3 + H_2O$$

$$H_2C{=}CHCH_2\dot{C}H_2\ (1\dot{C}_4H_7\text{-}4) \rightarrow C_2H_4 + \dot{C}_2H_3$$

$$a\dot{C}_3H_5 + H\dot{O}_2 \rightarrow \dot{O}H + \dot{C}_2H_3 + CH_2O$$

$$H_2C{=}CHCH{=}CH_2\ (1,3C_4H_6) + \dot{H} \rightarrow C_2H_4 + \dot{C}_2H_3$$

In the same manner the reaction

$$\dot{C}_2H_3 + \dot{H} \rightarrow C_2H_2 + H_2$$

has a positive sensitivity value because it removes C_2H_3 and a reactive H-atom and replaces them with C_2H_2 and H_2. The fact that this reaction removes a H-atom from the system and competes with

$$\dot{H} + O_2 \rightarrow \dot{O} + \dot{O}H$$

contributes to its positive sensitivity coefficient. The latter reaction has a strong negative sensitivity value because it increases the radical concentration present by reacting H-atom with O_2 to produce two reactive radical species.

The reaction

$$H_2C{=}CHCH{=}CH_2\ (1,3C_4H_6) + \dot{O} \rightarrow \dot{C}H_2CHCHCHO + \dot{H}$$

also has positive sensitivity values due to the fact that it competes directly with the pathway by which $1,3C_4H_6$ leads to the formation of $\dot{C}_2H_3$ as described above.

For these reasons the chemistry of vinyl radical was scrutinized. 94% of all $\dot{C}_2H_3$ present was produced by cyclohexyl radical decomposing via $1\dot{C}_4H_7$-4 radical as described above. Of the total $\dot{C}_2H_3$ radical formed, 37% reacts with O_2 to produce two $H\dot{C}O$ molecules via CH_2O.

$$\dot{C}_2H_3 + O_2 \xrightarrow{37\%} H\dot{C}O + CH_2O$$

$$CH_2O + R \xrightarrow{97\%} H\dot{C}O + RH \qquad R = \dot{H}, \dot{O}, \dot{O}H, H\dot{O}_2, \dot{C}H_3$$

The $H\dot{C}O$ then reacts

$$H\dot{C}O + O_2 \xrightarrow{81\%} CO + H\dot{O}_2$$

$$H\dot{C}O + M \xrightarrow{18\%} CO + \dot{H} + M$$

This means that for every molecule of $\dot{C}_2H_3$ that passes through this pathway 1.62 molecules of $H\dot{O}_2$ are formed.

$H\dot{O}_2$ plays an important role in increasing the reactivity of the system and its reaction pathways are described later. Therefore the reaction

$$\dot{C}_2H_3 + O_2 \rightarrow H\dot{C}O + CH_2O$$

has a negative sensitivity coefficient value at 1667 K. However, at 1250 K its sensitivity coefficient is positive. This is due to the fact that at both temperatures two molecules of $H\dot{C}O$ are formed: one molecule initially as a direct product of the reaction and another as a decomposition product of CH_2O. At 1250 K the $H\dot{C}O$ decomposes as shown above with 81% reacting with O_2 to form CO and $H\dot{O}_2$. This competes with $H\dot{C}O$ decomposition to form the more reactive H-atom and CO. The analysis at 1667 K showed that only 51% of $H\dot{C}O$ reacted with O_2, with another 45% taking the route that produced a H-atom. These findings have a direct bearing on the reaction of $\dot{H} + O_2 \rightarrow \dot{O} + \dot{O}H$. At 1667 K not only is less O_2 being consumed but also more H-atom is being produced, and vice versa at 1250 K, hence, the negative value at 1667 K and the positive value at 1250 K.

The reaction

$$CH_2O + \dot{C}H_3 \rightarrow CH_4 + H\dot{C}O$$

has a negative sensitivity value at 1250 K. This is due to the fact that at this temperature this reaction competes with the less reactive combination of two methyl radicals to form ethane. At 1667 K the formation of ethane does not occur, hence, the almost negligible positive value.

The CO produced by the above reactions reacts with either $\dot{O}H$ or $H\dot{O}_2$ radicals to produce CO_2 plus $\dot{H}$ or $\dot{O}H$ radicals. The reactions of $H\dot{O}_2$ are slightly more complex and interesting. 66% of $H\dot{O}_2$ adds to $\dot{C}H_3$ to form $CH_3\dot{O} + \dot{O}H$ radicals. The $CH_3\dot{O}$ radical then decomposes to CH_2O + H-atom (80%) or $H\dot{O}_2$ (20%). CH_2O forms $H\dot{C}O$ radical, 81% of which yields $H\dot{O}_2$ radical. In this manner the $H\dot{O}_2$ concentration is maintained and $H\dot{O}_2$ radical continues to react with $\dot{C}H_3$ to form *two* reactive $\dot{H}$ and $\dot{O}H$ radicals.

$$\dot{C}H_3 + H\dot{O}_2 \xrightarrow{66\%} CH_3\dot{O} + \dot{O}H$$

$$CH_3\dot{O}(+ M) \xrightarrow{80\%} CH_2O + \dot{H}(+ M)$$

$$CH_3\dot{O} + O_2 \xrightarrow{19\%} CH_2O + H\dot{O}_2$$

The substantial amount of reactive radicals generated in this way explains the negative sensitivity values observed for the addition of $H\dot{O}_2$ to $\dot{C}H_3$ producing $CH_3\dot{O}$ and $\dot{O}H$ radicals. The positive sensitivity value of

$$\dot{C}H_3 + H\dot{O}_2 \xrightarrow{5\%} CH_4 + O_2$$

is due to the fact that it is in direct competition with the more favorable $H\dot{O}_2 + \dot{C}H_3$ pathway. Of the remaining $H\dot{O}_2$ 7% reacts with $a\dot{C}_3H_5$ to yield $\dot{O}H$ plus $\dot{C}_2H_3$ and CH_2O; 6% reacts with $H\dot{O}_2$ to produce H_2O_2 plus O_2. The majority of both $\dot{C}_2H_3$ and CH_2O will react or decompose to give $H\dot{O}_2$ with reactive radicals being produced as side products; O_2 is also a very reactive species. This further explains the negative sensitivity of reactions that promote the formation of species that break down to form $H\dot{O}_2$. For example, the reaction

$$\dot{C}H_3 + O_2 \rightarrow \dot{O}H + CH_2O$$

has negative values because it produces CH_2O and by association $H\dot{O}_2$.

At both temperatures the reaction

$$H\dot{O}_2 + H\dot{O}_2 \rightarrow H_2O_2 + O_2$$

has positive sensitivity coefficients, because two reactive $H\dot{O}_2$ radicals are removed from the system.

The other major pathway by which the $\dot{C}_2H_3$ radical decomposes is by

$$\dot{C}_2H_3 + O_2 \xrightarrow{56\%} \dot{C}H_2CHO + \dot{O}$$

This reaction has a high negative sensitivity coefficient and leads to increased reactivity at both 1250 and 1667 K, because two radicals are produced from one.

The reaction

$$\dot{C}H_2CHO + O_2 \xrightarrow{37\%} CH_2CO + H\dot{O}_2$$

shows a positive sensitivity coefficient at 1667 K and a negative sensitivity coefficient at 1250 K, Figure 19. Analysis of the system reveals that at 1250 K $\dot{C}H_2CHO$ is consumed at almost the same rate at which it is formed, with 37% decomposing via this reaction. Therefore, increasing the *A*-factor of this reaction has the direct effect of decreasing the $\dot{C}H_2CHO$ concentration and producing more CH_2CO and the reactive $H\dot{O}_2$. At 1667 K, however, $\dot{C}H_2CHO$ is not consumed as readily and, of the $\dot{C}H_2$-CHO that does react, only 4% takes this pathway, hence, the almost negligible positive value.

At 1250 K the decomposition reaction

$$\dot{C}H_2CHO \rightarrow \dot{C}H_3 + CO$$

has a positive sensitivity value because it competes with the reaction with O_2 that produces CH_2CO and $H\dot{O}_2$, which has a high negative sensitivity coefficient, as described above.

The reactions

$$H\dot{O}_2 + \dot{O}H \rightarrow H_2O + O_2$$

$$\dot{C}H_3 + \dot{C}H_3(+ M) \rightarrow C_2H_6(+ M)$$

$$a\dot{C}_3H_5 + \dot{H}(+ M) \rightarrow C_3H_6(+ M)$$

$$C_3H_6 + \dot{H} \rightarrow a\dot{C}_3H_5 + H_2$$

$$C_3H_6 + \dot{O}H \rightarrow a\dot{C}_3H_5 + H_2O$$

$$CH_2O + \dot{O}H \rightarrow H\dot{C}O + H_2O$$

all have positive sensitivity values. This can be explained by the fact that these reactions favor the consumption of reactive radicals and the formation of more stable species. In addition, reactions in which stables species compete with the fuel in H-atom abstraction reactions by radical species inhibit reactivity and also show positive sensitivity coefficients.

The reaction

$$\dot{C}H_3 + \dot{O}H \rightarrow CH_2* + H_2O$$

has a negative sensitivity where two radicals combine to form reactive CH_2* and H_2O.

The sensitivity coefficients for reactions added, in this study, to the original mechanism by Laskin et al. are shown in Figure 20. The large negative value for

$$\mathrm{MCH} \rightarrow \mathrm{CYCHEXRAD} + \dot{\mathrm{C}}\mathrm{H}_3$$

is due to the fact that it favors the formation of $\dot{C}_2H_3$ radical, which subsequently reacts with O_2 and produces $H\dot{O}_2$ radical. The importance of these species has been explained earlier. The reactions

$$\mathrm{MCH} + \dot{\mathrm{H}} \rightarrow \mathrm{MCH{-}R'} + \mathrm{H}_2$$

(MCHR′ = all methylcyclohexyl radicals)

$$\mathrm{MCH} + \dot{\mathrm{O}}\mathrm{H} \rightarrow \mathrm{MCH{-}R'} + \mathrm{H}_2\mathrm{O}$$

(MCHR′ = all methylcyclohexyl radicals)

$$\mathrm{MCH} + \mathrm{CH}_3\dot{\mathrm{O}} \rightarrow \mathrm{MCH{-}R1} + \mathrm{CH}_3\mathrm{OH}$$

$$\mathrm{MCH} + \dot{\mathrm{O}} \rightarrow \mathrm{MCH{-}R1} + \dot{\mathrm{O}}\mathrm{H}$$

have positive sensitivities due to the fact that they compete with the formation of the cyclohexyl radical.

Because the following reactions

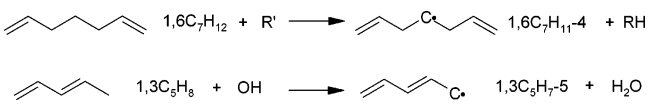

consume reactive radical species and produce stable products and resonantly stabilized radicals, they also have positive sensitivity coefficients.

The β-scission reactions of $1C_7H_{13}$-6 and eC_7H_{13}-a result in the formation of $1\dot{C}_4H_7$-4 radical:

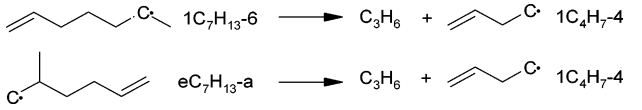

Because $1\dot{C}_4H_7$-4 radical decomposes to produce more than half of all the $\dot{C}_2H_3$ radical generated, the above reactions increase the reactivity of the system and have negative sensitivity coefficients.

The reaction

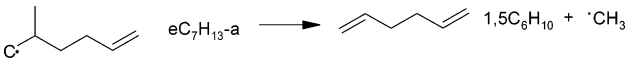

generates an alkene and a methyl radical and competes with the formation of $1\dot{C}_4H_7$-4 from $e\dot{C}_7H_{13}$-a, thereby reducing the reactivity of the system, resulting in a positive sensitivity coefficient for this reaction.

As before, a reaction that leads to the formation of a $\dot{C}_2H_3$ radical

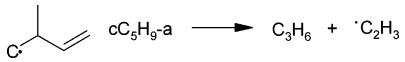

has a negative sensitivity coefficient.

Some other reactions

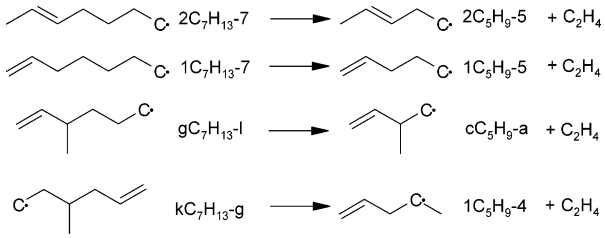

have large sensitivity coefficients. Analysis of reaction edits did not produce a clear picture of why these reactions had the observed sensitivities be they positive or negative. However, their sensitivity coefficients do not appear to be directly associated with the reactions themselves but can be attributed to the fact that these reactions are in competition with other pathways, which ultimately leads to an increase or a decrease in the reactivity of the system.

A sensitivity analysis was also performed for MCH oxidation in the flow reactor at 1815 ppm MCH, $\phi = 1.3$, 1160 K, and 1 atm, Figure 21. The sensitivity coefficient is defined as the percentage differences between the amount of MCH present at 1.375 ms (the time at which 10% fuel is consumed in the baseline mechanism) in the altered mechanism relative to the baseline mechanism, Figure 21. A negative sensitivity value signals an increase in the amount of MCH consumed. Reactions with a sensitivity value of less than 0.1% were excluded.

For the flow reactor sensitivity analysis increasing the *A*-factor for individual reactions in which H-atom abstracts H-atom from MCH causes the overall concentration of MCH present to fall in some cases and to increase in others, Figure 21. This is due to the stability of the decomposition products produced by the breakdown of the different $\dot{C}_7H_{13}$ radicals. However, it should be noted that the nature of the $\dot{C}_7H_{13}$ isomer formed does not change the sign of the sensitivity coefficient when a H-atom is abstracted by $\dot{O}H$, $\dot{O}$, $CH_3\dot{O}$, or $\dot{C}H_3$ radicals. Increasing the *A*-factor for all $\mathrm{MCH} + \dot{\mathrm{C}}\mathrm{H}_3 \rightarrow \mathrm{MCH{-}R'} + \mathrm{CH}_4$ causes an *increase* in the amount of MCH consumed. Conversely, increasing the *A*-factor for all H-atom abstractions from MCH by $\dot{O}H$, $\dot{O}$, $CH_3\dot{O}$ causes a *decrease* in the amount of MCH consumed. In general, it seems that increasing the *A*-factor of reactions that compete with the $\mathrm{MCH} \rightarrow \mathrm{CYCHEXRAD} + \dot{\mathrm{C}}\mathrm{H}_3$ reaction causes the system to be less reactive, resulting in a lower overall consumption of MCH. However, for some reactions, in particular some hydrogen atom abstractions from MCH by H-atoms and *all* hydrogen atom abstractions from MCH by $\dot{C}H_3$ radicals, the extra reactivity due to increasing the *A*-factor more than compensates for the fact that less MCH decomposes to give cyclohexyl radical and a $\dot{C}H_3$ radical.

For example, increasing the *A*-factor of H-atom abstraction by H-atom producing MCH-R1 or MCH-R4 causes an increase in the amount of MCH consumed at 1.375 ms. This occurs because MCH-R1 breaks down to produce one H-atom and other stable species, so there is no overall decrease in H-atom concentration. The same trend is observed when MCH-R4 is produced. 85% of the MCH-R4 goes to $1\dot{C}_4H_7$-4, which gives $1,3C_4H_6$ and a H-atom. Another 5% goes to C_3H_6 and a H-atom. In summary, 90 ± 7% of MCH-R4 that breaks down via this path produces one H-atom, keeping the overall H-atom supply almost constant.

Conversely, increasing the rates of H-atom abstractions by H-atom forming CYCHEXCH2, MCH-R2, or MCH-R3 results in a decrease in the amount of MCH consumed at 1.375 ms. Of the CYCHEXCH2 formed 60% produces allyl ($a\dot{C}_3H_5$) radical and two ethylene (C_2H_4) molecules, and 40% produces buta-1,3-diene ($1,3C_4H_6$), C_2H_4, and a $\dot{C}H_3$ radical. A methyl

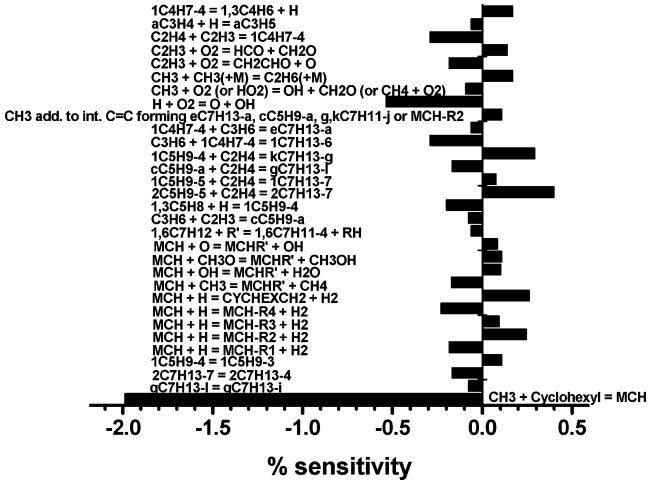

Figure 21. Sensitivity analysis, to MCH concentration at 1.375 ms, for flow reactor oxidation at 1815 ppm MCH, $\phi = 1.3$, 1160 K, and 1 atm. (MCHR′ = all methylcyclohexyl radicals.)

radical is less reactive than a H-atom because only 19% of methyl radicals consume the fuel via H-atom abstraction, compared to 89% of the H-atoms produced. Through these routes the reactive radical pool decreases. MCH-R2 decomposes to give three main types of products:

1. 8% MCH-R2 gives $i\dot{C}_5H_8$ and C_2H_5 and 18% gives $1,3C_5H_8$ and $\dot{C}_2H_5$ radical, with $\dot{C}_2H_5$ radical undergoing β-scission to yield C_2H_4 and a H-atom. This is the only major MCH-R2 decomposition pathway that would speed up the rate of decomposition of MCH.

2. 43% of MCH-R2 gives $1,3C_4H_6$ and a $\dot{C}H_3$ radical, which is much less reactive than a H-atom.

3. An additional 9% of MCH-R2 breaks down to form two C_2H_4 molecules and a $\dot{C}_2H_3$ radical. 91% of $\dot{C}_2H_3$ reacts with O_2 to form different species, with only 9% undergoing β-scission to produce ethylene and a hydrogen atom.

All other pathways by which MCH-R2 and its subproducts decomposed yielded stable intermediates such as $1,3C_4H_6$, C_2H_4, $1,3C_5H_8$, and iC_5H_8, with negligible amounts of H-atom being formed. In summary, for every one hundred H-atoms used for hydrogen abstraction forming MCH-R2, less than thirteen were returned to the cycle. 55% of MCH-R3 breaks down via pathways that produce a H-atom. The other pathways produce more stable species. Therefore, increasing the rate of H-atom abstraction by H-atom forming MCH-R3 leads to an overall decrease in H-atom concentration, as only half the H-atoms consumed in abstraction from MCH are replaced.

Increasing the rates for H-atom abstraction by $\dot{O}H$, $CH_3\dot{O}$, and $\dot{O}$ radicals leads to a decrease in the amount of MCH consumed. These reactions compete with the decomposition of MCH forming cyclohexyl and a methyl radical. As described previously, because this latter reaction shows a high negative sensitivity coefficient, any reaction that competes with it will show a positive sensitivity, as observed.

Increasing the rate of hydrogen atom abstraction by $\dot{C}H_3$ radicals causes MCH consumption to increase. This is because $\dot{H}$ abstraction is competing with the methyl plus methyl radical recombination to form ethane. Increasing H abstraction will lead to fuel decomposition plus a stable CH_4 molecule, instead of a stable C_2H_6 molecule with no MCH decomposition.

Conclusions

Ignition delay times have been measured for 0.5% MCH plus 10.5% O_2 ($\phi = 0.5$), 1.0% MCH plus 10.5% O_2 ($\phi = 1.0$), and 1.0% MCH plus 5.25% O_2 ($\phi = 2.0$) mixtures in Ar, Figures 7 and 8. These experiments were carried out behind reflected shock waves at reflected shock pressures of 1.0, 2.0, and 4.0 atm across a temperature range of 1200−2200 K. As expected, the ignition delay times for a particular mixture decreased as the reflected shock pressure was increased from 1.0 to 2.0, and 4.0 atm. Increasing the O_2 concentration in the mixture from 5.25 to 10.5%, while maintaining a constant MCH concentration of 1.0%, caused a large decrease in the ignition delays times observed. On the other hand, increasing the fuel concentration from 0.5 to 1.0%, while keeping the O_2 constant at 10.5%, caused a lengthening in the ignition delay times observed. This change was about one-third of that observed when the O_2 concentration was changed. The experimental conditions studied previously by Hawthorne and Nixon[40] were replicated. The ignition delay times measured agreed well with the previous work, Figure 6.

A detailed kinetic model was created consisting of 190 species and 904 reversible reactions. The model predictions are in good agreement with the shock tube ignition delay times. The general trends displayed by the experimental data, such as changes in ignition delay times due to different reflected shock temperatures and pressure as well as different fuel and O_2 concentrations, were also reflected by the simulated delay times. The model was also used to simulate species profiles produced for MCH oxidation and pyrolysis in a turbulent flow reactor study by Zeppieri et al.,[39] Figures 10 and 11. In both cases the model agrees with the profiles of the MCH decomposition products buta-1,3-diene, isoprene, ethylene, and propene. There is an underestimation of the amount of methane produced and the simulated MCH decomposition profile does not decrease as rapidly as the experimental data. To allow for the experimental uncertainties of the time−temperature history of the in-flowing reactants, and to give the best overall agreement between the simulated and experimental species profiles, the simulated pyrolysis data was time-shifted by −5 ms; no time shifting was carried out on the oxidation profiles. Some species predicted by the model were not observed under the oxidation experimental conditions; in the cases of hydrogen, water, and formaldehyde this may have been due to the experimental setup used to carry out species analysis, Figure 12. Measurable quantities of penta-1,3-diene were predicted by the model, but this species was not reported in the experiments, Figure 11.

Finally, sensitivity studies show that MCH oxidation is very sensitive to ethylene/vinyl chemistry, indicating that an extensively validated detailed chemical kinetic mechanism for this fuel is vital to accurately simulate MCH oxidation.

Acknowledgment. J.P.O. thanks Enterprise Ireland (SC/2001/313) and Mayo County Council for financial assistance. The assistance of the Environmental Change Institute and the Higher Education Authority (PRTLI Cycle 2) is also gratefully acknowledged. We thank Dr. William Pitz (Lawrence Livermore National Laboratory) for helpful discussions.

References and Notes

(1) Simmie, J. M. *Prog. Energy Combust. Sci.* **2003**, *29*, 599−634.

(2) Goloniva, E. S.; Fyodorov, G. G. *Proc. Combust. Inst.* **1956**, *6*, 88−96.

(3) Bittner, J. D.; Howard, J. B. *Proc. Combust. Inst.* **1981**, *18*, 1106−1116.

(4) Lovell, A. B.; Brezinsky, K.; Glassman, I. *Proc. Combust. Inst.* **1988**, *22*, 1063−1074.
(5) Emdee, J. L.; Brezinsky, K.; Glassman, I. *J. Phys. Chem.* **1992**, *96*, 2151−2161.
(6) Lindstedt, R. P.; Skevis, G. *Combust. Flame* **1994**, *99*, 551−561.
(7) Zhang, H. Y.; McKinnon, J. T. *Combust. Sci. Technol.* **1995**, *107*, 261−300.
(8) Tan, Y.; Frank, P. *Proc. Combust. Inst.* **1996**, *26*, 677−684.
(9) Davis, S. G.; Wang, H.; Brezinsky, K.; Law, C. K. *Proc. Combust. Inst.* **1996**, *26*, 1025−1033.
(10) Chai, Y.; Pfefferle, L. D. *Fuel* **1998**, *77*, 313−320.
(11) Alzueta, M. U.; Glarborg, P.; Dam-Johansen, K. *Int. J. Chem. Kinet.* **2000**, *32*, 498−522.
(12) Schöbel, A. *Experimentelle und numerische Untersuchung des Benzolabbaus im Strömungsreaktor bei mittleren Temperaturen*, 2000 Wiss. Berichte FZKA 6498, Forschungszentrum Karlsruhe.
(13) Ristori, A.; Dagaut, P.; El Bakali, A.; Pengloan, G.; Cathonnet, M. *Combust. Sci. Technol.* **2001**, *167*, 223−256.
(14) Lindstedt, R. P.; Maurice, L.; Meyer, M. *Faraday Discuss.* **2001**, *119*, 409−432.
(15) Richter, H.; Howard, J. B. *Phys. Chem. Chem. Phys.* **2002**, *4*, 2038−2055.
(16) Da Costa, I.; Fournet, R.; Billaud, F.; Battin-Leclerc, F. *Int. J. Chem. Kinet.* **2003**, *35*, 503−524.
(17) Brezinsky, K. *Prog. Energy Combust. Sci.* **1986**, *12*, 1−24.
(18) Pamidimukkala, K. M.; Kern, R. D.; Patel, M. R.; Wei, H. C.; Kiefer, J. H. *J. Phys. Chem.* **1987**, *91*, 2148−2154.
(19) Braun-Unkhoff, M.; Frank, P.; Just, Th. *Proc. Combust. Inst.* **1988**, *22*, 1053−1061.
(20) Lindstedt, R. P.; Maurice, L. Q. *Combust. Sci. Technol.* **1996**, *120*, 119−167.
(21) Klotz, S. D.; Brezinsky, K.; Glassman, I. *Proc. Combust. Inst.* **1998**, *27*, 337−344.
(22) Pengloan, G.; Dagaut, P.; Djebaïli-Chaumeix, N.; Paillard, C. E.; Cathonnet, M. *Colloq. Combust. Propre, Orléans* **2001**, p 9.
(23) Dagaut, P.; Pengloan, G.; Ristori, A. *Phys. Chem. Chem. Phys.* **2002**, *4*, 1846−1854.
(24) Sivaramakrishnan, R.; Tranter, R. S.; Brezinsky, K.; Durgam, S.; Vasudevan, H. *Proc. Joint Mtg. U. S. Sect. Combust. Inst., 3rd* **2003**, A04.
(25) Ribaucour, M.; Roubaud, A.; Minetti, R.; Sochet, L. R. *Proc. Combust. Inst.* **2000**, *28*, 1701−1707.
(26) Roubaud, A.; Minetti, R.; Sochet, L. R. *Combust. Flame* **2000**, *121*, 535−541.
(27) Roubaud, A.; Lemaire, O.; Minetti, R.; Sochet, L. R. *Combust. Flame* **2000**, *123*, 561−571.
(28) Dagaut, P.; Ristori, A.; El Bakali, A.; Cathonnet, M. *Fuel* **2002**, *81*, 173−184.
(29) Lemaire, O.; Ribaucour, M.; Carlier, M.; Minetti, R. *Combust. Flame* **2001**, *127*, 1971−1980.
(30) Ribaucour, M.; Lemaire, O.; Minetti, R. *Proc. Combust. Inst.* **2002**, *29*, 1303−1310.
(31) Dayma, G.; Glaude, P. A.; Fournet, R.; Battin-Leclerc, F. *Int. J. Chem. Kinet.* **2003**, *35* (7), 273−285.
(32) http://www.faqs.org/faqs/autos/gasoline-faq/part1/preamble/html.
(33) Yu, J.; Eser, S. *Ind. Eng. Chem. Res.* **1995**, *34*, 404−409.
(34) Violi, A.; Yan, S.; Eddings, E. G.; Sarofim, A. F.; Granata, S.; Faravelli, T.; Ranzi, E. *Combust. Sci. Technol.* **2002**, *174*, 399−417.
(35) Maurice, L.; Edwards, T.; Griffiths, J. *Prog. Astronaut. Aeronaut.* **2000**, *189*, 757−822.
(36) Tanaka, S.; Ayala, F.; Keck, J. C.; Heywood, J. B. *Combust. Flame* **2003**, *132*, 219−239.
(37) Owen, K.; Cooley, T. *Automotive Fuels Reference Book*, 2nd ed.; Society of Automotive Engineers: Warrendale, PA, 1995; p 831.
(38) Brown, T. C.; King, K. D. *Int. J. Chem. Kinet.* **1989**, *21*, 251−266.
(39) Zeppieri, S.; Brezinsky, K.; Glassman, I. *Combust. Flame* **1997**, *108*, 266−286.
(40) Hawthorn, R. D.; Nixon, A. C. *AIAA* **1966**, *4*, 513−520.
(41) Granata, S.; Faravelli, T.; Ranzi, E. *Combust. Flame* **2003**, *132*, 533−544.
(42) Ranzi, E.; Gaffuri, P.; Faravelli, T.; Dagaut, P. *Combust. Flame* **1995**, *103*, 91−106.
(43) Ranzi, E.; Faravelli, T.; Gaffuri, P.; Sogaro, A.; D'Anna, A.; Ciajolo, A. *Combust. Flame* **1997**, *108*, 24−42.
(44) Ranzi, E.; Dente, M.; Goldaniga, A.; Bozzano, G.; Faravelli, T. *Prog. Energy Combust. Sci.* **2001**, *27*, 99−139.
(45) Ben-Dor, G.; Igra, O.; Elperin, T.; Lifhitz, In. A. *Handbook of Shock Waves*; Academic Press: New York, 2001; Vol. 3, pp 212−256.
(46) Morley, C. http://www.gaseq.co.uk/.
(47) Smith, J. M. Ph.D. Thesis, National University of Ireland, Galway, 2004.
(48) Michael, J. V.; Sutherland, J. W. *Int. J. Chem. Kinet.* **1986**, *18*, 409−436.
(49) Horning, D. C.; Davidson, D. F.; Hanson, R. K. *Int. Symp. Shock Waves*, *23rd* **2001**, paper 5732.
(50) Horning, D. C.; Davidson, D. F.; Hanson, R. K. *J. Propul. Power* **2002**, *18*, 363−371.
(51) Kee, R. J.; Rupley, F. M.; Miller, J. A.; Coltrin, M. E.; Grcar, J. F.; Meeks, E.; Moffat, H. K.; Lutz, A. E.; Dixon-Lewis, G.; Smooke, M. D.; Warnatz, J.; Evans, G. H.; Larson, R. S.; Mitchell, R. E.; Petzold, L. R.; Reynolds, W. C.; Caracotsios, M.; Stewart, W. E.; Glarborg, P.; Wang, C.; Adigun, O.; Houf, W. G.; Chou, C. P.; Miller, S. F. *Chemkin Collection*, Release 3.7; Reaction Design, Inc.: San Diego, CA, 2002.
(52) Laskin, A.; Wang, H.; Law, C. K. *Int. J. Chem. Kinet.* **2000**, *32*, 589−614.
(53) Ó Conaire, M.; Curran, H. J.; Simmie, J. M.; Pitz, W. J.; Westbrook, C. K. *Int. J. Chem. Kinet.* **2004**, *36*, 603−622.
(54) Curran, H. J.; Gaffuri, P.; Pitz, W. J.; Westbrook, C. K. *Combust. Flame* **1998**, *114*, 149−177.
(55) Curran, H. J.; Gaffuri, P.; Pitz, W. J.; Westbrook, C. K. *Combust. Flame* **2002**, *129*, 253−280.
(56) Prosen, E. J.; Johnson, W. H.; Rossini, F. D. *J. Res. Natl. Bur. Stand.* **1946**, *37*, 51−56.
(57) Beckett, C. W.; Pitzer, K. S.; Spitzer, R. *J. Am. Chem. Soc.* **1947**, *69*, 2488−2495.
(58) Ritter, E. R.; Bozzelli, J. W. *Int. J. Chem. Kinet.* **1991**, *23*, 767−778.
(59) Benson, S. W. *Thermochemical Kinetics*; John Wiley and Sons: New York, 1976.
(60) Lay, T.; Bozzelli, J. W.; Dean, A. M.; Ritter, E. R. *J. Phys. Chem.* **1995**, *99* (39), 14514−14527.
(61) Sumathi, R.; Green, W. H., Jr. *Phys. Chem. Chem. Phys.* **2003**, *5*, 3402−3417.
(62) O'Neal, H. E.; Benson, S. W. *J. Phys. Chem.* **1967**, *71* (9), 2903−2921.
(63) Tsang, W. *J. Phys. Chem. Ref. Data* **1990**, *19*, 1−68.
(64) Westbrook, C. K.; Pitz, W. J.; Curran, H. J.; Boercker, J.; Kunrath, E. *Int. J. Chem. Kinet.* **2001**, *33*, 868−877.
(65) Curran, H. J. *Int. J. Chem. Kinet.*, in press.
(66) Matheu, D. M.; Green, W. H., Jr.; Grenda, J. M. *Int. J. Chem. Kinet.* **2003**, *35*, 95−119.
(67) Solomons, T. W. Graham *Organic Chemistry*, 6th ed.; Wiley: New York, 1996; p 145.
(68) Pine, S. H. *Organic Chemistry*, 5th ed.; McGraw-Hill: New York, 1987; p 547.
(69) Orchard, S. E.; Thrush, B. A. *Proc. R. Soc. London A* **1974**, *337*, 257−274.
(70) Alfassi, Z. B.; Benson, S. W.; Golden, D. M. *J. Am. Chem. Soc.* **1973**, *95*, 4784−4788.
(71) Dean, A. M. *J. Phys. Chem.* **1985**, *89*, 4600−4608.
(72) Weissman, M. A.; Benson, S. W. *J. Phys. Chem.* **1988**, *92*, 4080−4084.
(73) Nicovich, J. M.; Ravishankara, A. R. *J. Phys. Chem.* **1984**, *88*, 2534−2541.
(74) Lewis, D. K.; Bergmann, J.; Manjoney, R.; Paddock, R.; Kaira, B. L. *J. Phys. Chem.* **1984**, *88*, 4112−4116.
(75) Hidaka, Y.; Chimori, T.; Shiba, S.; Suga, M. *Chem. Phys. Lett.* **1984**, *111*, 181−183.
(76) Skinner, G. B.; Rogers, D.; Patel, K. B. *Int. J. Chem. Kinet.* **1981**, *13*, 481−495.
(77) Newman, C. G.; O'Neal, H. E.; Ring, M. A.; Leska, F.; Shipley, N. *Int. J. Chem. Kinet.* **1979**, *11*, 1167−1182.
(78) Barnard, J. A.; Parrott, T. K. *J. Chem. Soc., Faraday Trans.* **1976**, *1:72*, 2404−2415.
(79) Tsang, W. *Int. J. Chem. Kinet.* **1973**, *5*, 651−662.
(80) Tsang, W. *Int. J. Chem. Kinet.* **1970**, *2*, 311−323.
(81) Fahr, A.; Stein, S. E. *Proc. Combust. Inst.* **1988**, *22*, 1023−1029.
(82) Newcomb, M. *Tetrahedron* **1993**, *49*, 1151−1176.
(83) Brezinsky, K.; Litzinger, T. A.; Glassman, I. *Int. J. Chem. Kinet.* **1984**, *16*, 1053−1074.